

ER 1356

CORRELATION BY DIMENSIONAL ANALYSIS OF  
BREAKTHROUGH CURVES IN FIXED-BED ADSORPTION SYSTEMS

by

Mahir Jalili

ARTHUR LAKES LIBRARY  
COLORADO SCHOOL OF MINES  
GOLDEN, COLORADO

ProQuest Number: 10781081

All rights reserved

INFORMATION TO ALL USERS

The quality of this reproduction is dependent upon the quality of the copy submitted.

In the unlikely event that the author did not send a complete manuscript and there are missing pages, these will be noted. Also, if material had to be removed, a note will indicate the deletion.



ProQuest 10781081

Published by ProQuest LLC (2018). Copyright of the Dissertation is held by the Author.

All rights reserved.

This work is protected against unauthorized copying under Title 17, United States Code  
Microform Edition © ProQuest LLC.

ProQuest LLC.  
789 East Eisenhower Parkway  
P.O. Box 1346  
Ann Arbor, MI 48106 – 1346

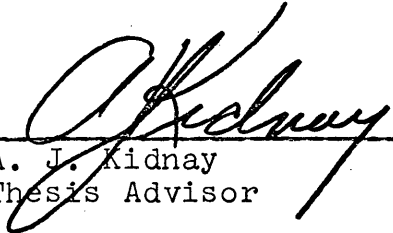
A Thesis submitted to the Faculty and the Board of Trustees of the Colorado School of Mines in partial fulfillment of the requirements for the degree of Master of Engineering in Chemical and Petroleum-Refining Engineering.

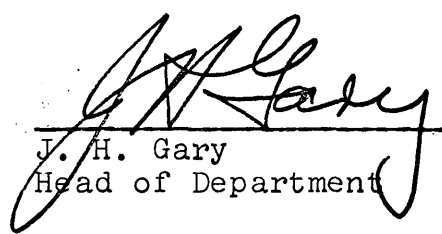
Signed: Mahir Talib

Golden, Colorado

Date: Jan 22, 1971

Approved: \_\_\_\_\_

  
A. J. Kidney  
Thesis Advisor

  
J. H. Gary  
Head of Department

Golden, Colorado

Date: Jan 22, 1971

ARTHUR LAKES LIBRARY  
COLORADO SCHOOL OF MINES  
GOLDEN, COLORADO

## ABSTRACT

Dimensional analysis is employed in correlating the breaktimes of several breakthrough curves. The treatment assumed that all of the transfer resistance lies in the gas phase.

The breakthrough curves used to develop the correlation were all for cryogenic systems: 1) methane-hydrogen, nitrogen-hydrogen, methane-helium, and nitrogen-helium on activated charcoal at  $76^{\circ}\text{K}$ ; 2) methane-hydrogen, and nitrogen-hydrogen on synthetic zeolite at  $76^{\circ}\text{K}$ .

The correlation is tested on three systems: methane-hydrogen on silica gel at  $-115^{\circ}\text{F}$ , water-air on activated alumina at  $80^{\circ}\text{F}$ , and water-air on molecular sieves at  $90^{\circ}\text{F}$ . The predicted breaktimes for these systems are in good agreement with the actual values, from an engineering consideration.

ARTHUR LAKES LIBRARY  
COLORADO SCHOOL OF MINES  
GOLDEN, COLORADO

Dedicated to

Marwan, Thuwayba, and Mazin

## TABLE OF CONTENTS

	Page
ABSTRACT. . . . .	iii
DEDICATION. . . . .	iv
LIST OF FIGURES . . . . .	vi
ACKNOWLEDGMENTS . . . . .	viii
INTRODUCTION. . . . .	1
BACKGROUND. . . . .	3
PREDICTION OF BREAKTHROUGH CURVES . . . . .	8
DIMENSIONAL ANALYSIS. . . . .	12
CORRELATION . . . . .	15
RESULTS . . . . .	62
DISCUSSION OF RESULTS . . . . .	70
CONCLUSIONS . . . . .	74
NOTATION. . . . .	76
LITERATURE CITED. . . . .	78

## LIST OF FIGURES

Figure	Page
1. Fixed-Bed Adsorber . . . . .	4
2. The Adsorption Wave. . . . .	6
3. Breakthrough Curves for Methane-Hydrogen on Charcoal. . . . .	16
4. Breakthrough Curves for Methane-Hydrogen on Charcoal. . . . .	17
5. Breakthrough Curves for Nitrogen-Hydrogen on Charcoal. . . . .	18
6. Breakthrough Curves for Nitrogen-Hydrogen on Charcoal. . . . .	19
7. Breakthrough Curves for Methane-Helium on Charcoal. . . . .	20
8. Breakthrough Curves for Methane-Helium on Charcoal. . . . .	21
9. Breakthrough Curves for Nitrogen-Helium on Charcoal. . . . .	22
10. Breakthrough Curves for Nitrogen-Helium on Charcoal. . . . .	23
11. Instantaneous-Breakthrough Correlation for the Charcoal Systems . . . . .	29
12. Schmidt Number Versus Pressure for Hydrogen. . .	40
13. Determination of the Exponent of $\rho_B/\rho$ . . . . .	43
14. Determination of the Exponent of $Re$ . . . . .	46
15. Determination of the Exponent of $v$ . . . . .	48
16. Determination of the Exponent of $Sc$ . . . . .	51
17. Mass Transfer Correlation. . . . .	53

Figure	Page
18. Determination of the Exponent of $Q/D_p^3$ . . . . .	55
19. The Breaktime Correlation. . . . .	61
20. Instantaneous-Breakthrough Correlation for the Synthetic Zeolite Systems. . . . .	72

ACKNOWLEDGMENTS

The author wishes to thank his thesis advisor, Dr. Arthur J. Kidnay, for his tremendous help and encouragement. Appreciation is extended to Dr. John O. Golden, and Professor William R. Astle, for serving as committee members.

The author also wishes to thank Dr. Lee C. Eagleton, Head of the Chemical Engineering Department at the Pennsylvania State University, for his help.

## INTRODUCTION

In fixed-bed adsorption two mass transfer processes take place: the diffusion through the gas phase, and diffusion into the solid particle. If both of these processes were instantaneous, a plot of the adsorber outlet concentration versus time would be a step function. Usually, however, one or both processes are relatively slow, with the result that the breakthrough curve assumes an S shape.

The design of a fixed-bed adsorber, and the prediction of the length of the adsorption cycle between reactivation, requires knowledge of the percentage approach to saturation at the breakpoint (the point when the adsorber outlet concentration reaches an appreciable value). This in turn requires the designer to predict the time of the breakpoint (breaktime) and the shape of the breakthrough curve. The unsteady-state circumstances of fixed-bed adsorption and the many factors which influence the phenomenon make such computations for the general case most formidable problems. Therefore, in planning new adsorption processes, the breakpoint and the breakthrough curve for a particular system are usually determined experimentally under conditions resembling as much as possible those to be encountered in the process.

In this engineering report, the breaktimes for all breakthrough curves are correlated on a single plot, with

the use of dimensional analysis, in a manner similar to heat-transfer or mass-transfer correlations. The breakpoint is arbitrarily chosen to correspond to a value of  $C/C_0$  of 0.1.

## BACKGROUND

### Physical Adsorption

Physical adsorption is the physical transfer of a solute in a gas or liquid to a solid surface where the solute is held as a result of intermolecular attraction with the solid's molecules. The adsorbed solute does not dissolve in the solid but remains on the solid surface or in the pores of the solid. Adsorption is reversible so that by changing pressure or temperature, the solute may be removed from the solid. At equilibrium, the adsorbed solute has a partial pressure equal to the partial pressure of the contacting fluid phase, and by lowering the pressure of the gas phase or by raising the temperature, the adsorbed solute is readily removed.

### Fixed-Bed Adsorption

Owing to the inconvenience and relatively high cost of continuously transporting solid particles as required in steady-state operation, it is frequently found more economical to pass the fluid mixture to be treated through a stationary bed of adsorbent. As increasing amounts of fluid are passed through such a bed, the solid adsorbs increasing amounts of solute and an unsteady-state prevails. A schematic of a fixed-bed adsorber, and the plot of  $C$ , concentration of the fluid phase leaving the adsorber, versus time (breakthrough curve) are shown in Figure 1.

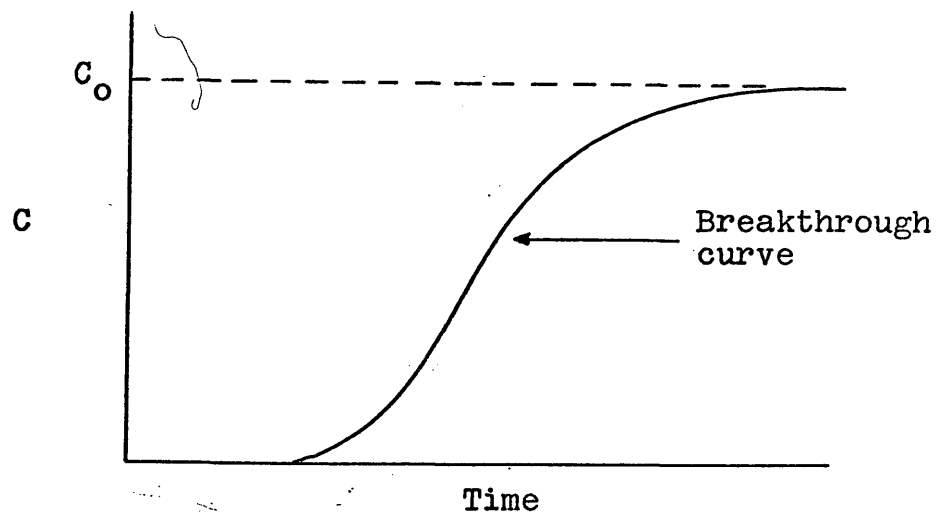
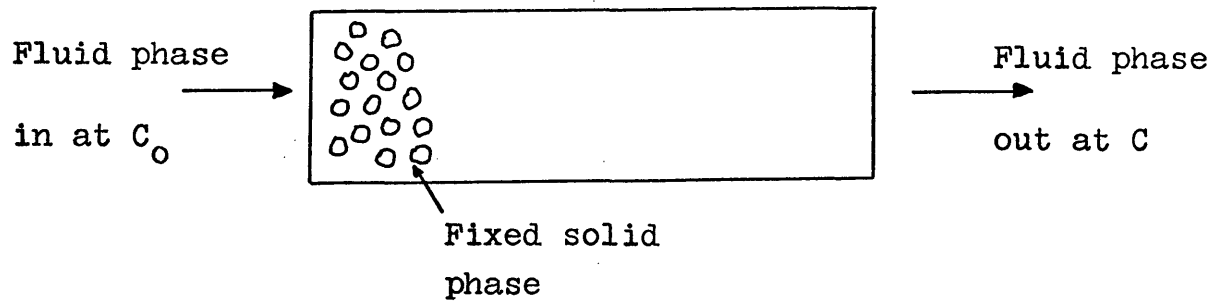


Figure 1. Fixed-Bed Adsorber

This technique is very widely used and finds application in such diverse fields as the recovery of valuable solvent vapor from gases, purification of gases prior to liquefaction, dehydration of gases and liquids, decolorizing mineral and vegetable oils, and many others.

Consider the case of a binary solution, either gas or liquid, containing a strongly adsorbed solute at concentration  $C_0$ . The fluid is to be passed continuously down through a relatively deep bed of adsorbent initially free of adsorbate. The uppermost layer of solid, in contact with the strong solution entering, at first adsorbs solute rapidly and effectively, and what little solute is left in the solution is substantially all removed by the layers of solid in the lower part of the bed. The effluent from the bottom of the bed is practically solute-free as at  $C_a$  in the lower part of Figure 2 (Treybal, 1955, p. 499). The distribution of the adsorbate in the solid bed is indicated in the sketch in the upper part of this figure at (a), where the relative density of the horizontal lines in the bed is meant to indicate the relative concentration of the adsorbate. The uppermost layer of the bed is practically saturated, and the bulk of the adsorption takes place over a relatively narrow adsorption zone in which the concentration changes rapidly, as shown. As the solution continues to flow, the adsorption zone moves downward as a wave, at a rate ordinarily very much more slowly than the linear velocity of the

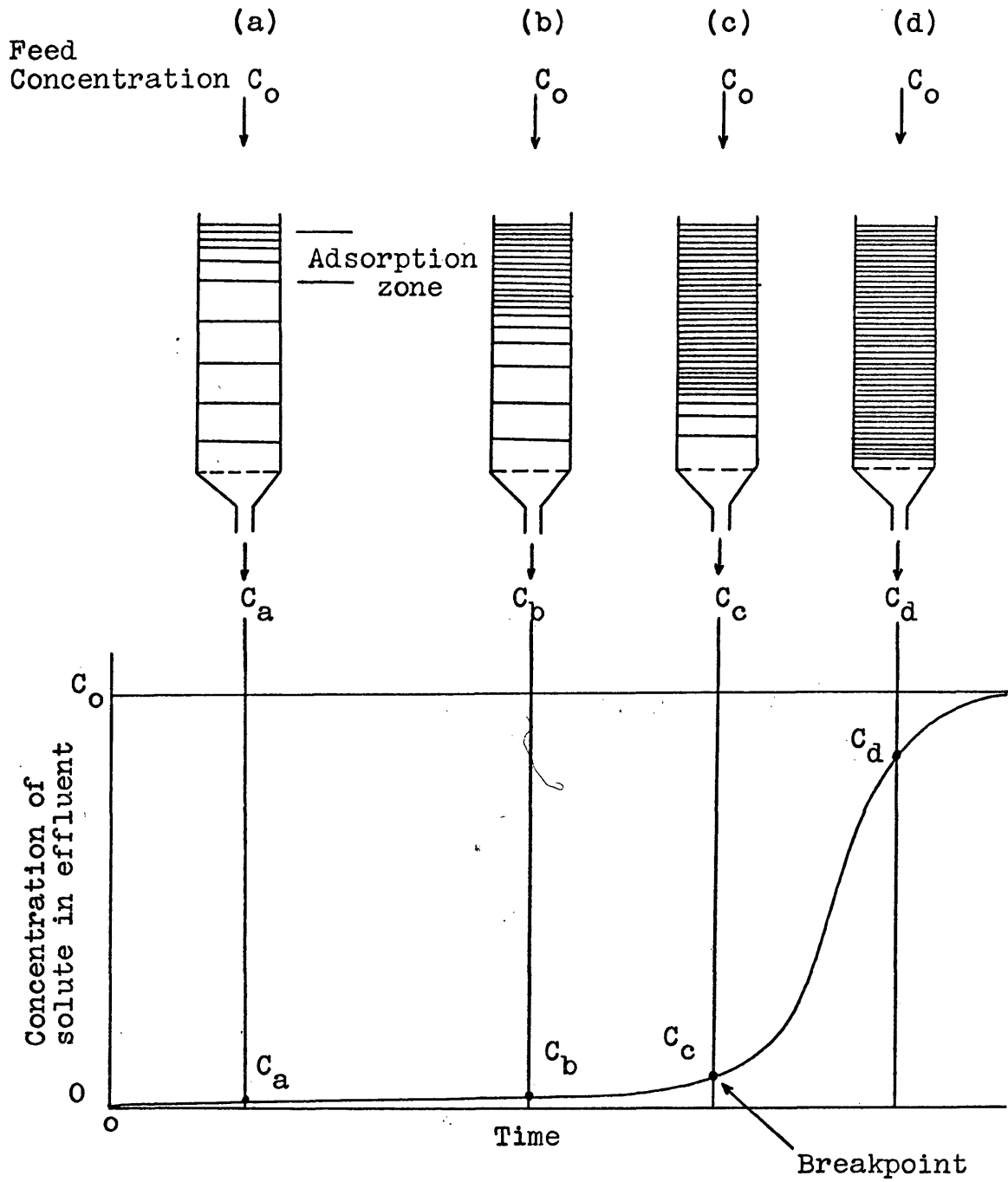


Figure 2. The Adsorption Wave

fluid through the bed. At a later time, as at (b), roughly half the bed is saturated with solute, but the effluent concentration  $C_b$  is still substantially zero. At (c), the lower portion of the adsorption zone has just reached the bottom of the bed, and the concentration of solute in the effluent has suddenly risen to an appreciable value  $C_c$  for the first time. The system is said to have reached the "breakpoint." The solute concentration in the effluent now rises rapidly as the adsorption zone passes through the bottom of the bed and at (d) has substantially reached the initial value  $C_o$ . The portion of the effluent concentration curve between positions (c) and (d) is termed the "break-through" curve. If solution continues to flow, little additional adsorption takes place since the bed is for all practical purposes entirely in equilibrium with the feed solution.

The shape and the time of appearance of the breakthrough curve influence greatly the method of operating a fixed-bed adsorber. The curves generally have an S shape, but they may be steep or relatively flat and in some cases considerably distorted. The actual rate and mechanism of the adsorption process, the nature of adsorption equilibrium, the fluid velocity, the concentration of the solute in the feed, and the length of the adsorber bed all contribute to the shape of the curve produced for any system.

## PREDICTION OF BREAKTHROUGH CURVES

The mathematical treatment of the breakthrough curve is a subject that has received considerable attention, but the problem is so complex that no general solution has yet been attained. A wide variety of equations for the breakthrough curve has been developed; Klotz (1946, p. 241) summarizes the work prior to 1946, while references to more recent work can be found in Vermeulen (1958, p. 147), and Hall, Eagleton, Acrivos, and Vermeulen (1966, p. 212). Most of the methods that have been developed assume that all of the transfer resistance lies in either the gas phase or the adsorbed phase, or are rather limited in the type of adsorption isotherm they can treat. Of the various methods that allow for transfer resistances in both phases, the method of Eagleton and Bliss (1953, p. 543) is probably the best from an engineering consideration, since it treats gas adsorption in a manner completely analogous to gas absorption and does not require curve matching or numerical integration in order to evaluate the coefficients.

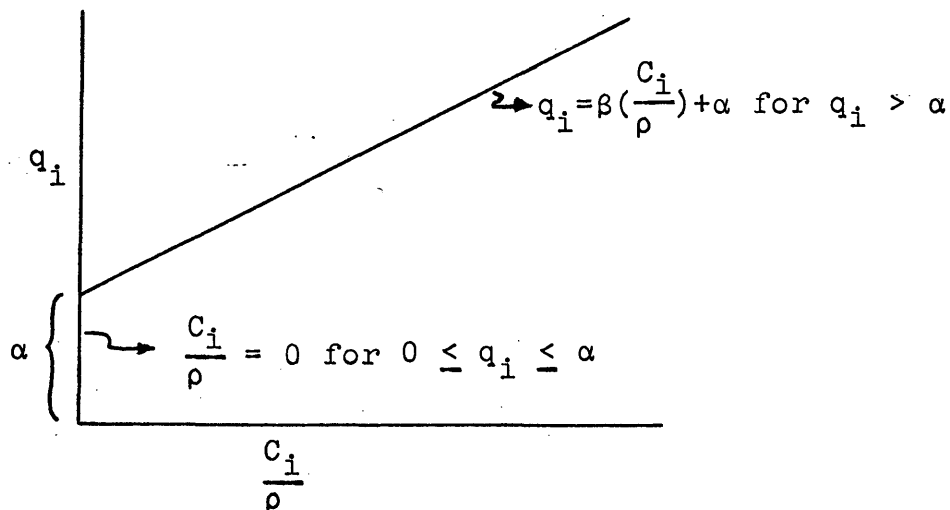
The Method of Eagleton and Bliss: This is taken from Eagleton's Ph.D. thesis (1951, p. 10). It begins with the following assumptions:

- 1) Constant inlet concentration and flow rate.
- 2) No radial concentration or pressure gradients.
- 3) Isothermal operation.
- 4) No axial diffusion.
- 5) The length of the mass transfer zone remains constant as it moves through the adsorbent bed.
- 6) Only the trace component is adsorbed.
- 7) The rate equation is

$$\left(\frac{dq}{dt}\right)_l = \frac{k_g S}{\rho} (C - C_i) = k_s S (q_i - q)$$

A linear driving force is used for diffusion into the pores, rather than Fick's second law, in order to simplify the mathematics.

- 8) The adsorption isotherm can be approximated by two straight lines, as shown below.



With these assumptions, they develop the following equations for the breakthrough curve.

for  $C < C_d$

$$\ln \frac{C}{C_o} = + \frac{C_o k_g S}{\rho q_o} t - \frac{k_g S X}{V} - 2 + \frac{C_o}{C_d} + \ln \left( \frac{C_d}{C_o} \right),$$

for  $C > C_d$

$$\ln (1 - C/C_o) = - \left\{ \frac{C_d/C_o}{1 - C_d/C_o} \right\} \left\{ \frac{C_o k_g S}{\rho q_o} t - \frac{k_g S X}{V} - 2 + \frac{C_o}{C_d} \right\} + \ln \{1 - C_d/C_o\}$$

$C_d$  is the gas phase concentration at the point of discontinuity in the isotherm, i.e. when  $q_i = \alpha$ , and is obtained from the equation

$$C_d = \frac{\alpha}{\frac{q_o}{C_o} - r}$$

where

$$r = \frac{-k_g S}{k_s S}$$

Kidnay (1968, p. 103) predicted a number of breakthrough curves using the above equations. The predicted curves demonstrate that the breakthrough curves can be predicted fairly well.

Engel and Coull Method: An empirical method of correlating breakthrough curves was developed by Engel and Coull (1942, p. 947), who noted that the breakthrough curve closely resembles the probability integral or error curve,

and thus proposed the equation

$$\frac{C_o - C}{C_o} = 0.5 \left\{ 1 + \frac{2}{\sqrt{\pi}} \int_0^z e^{-z^2} dz \right\}$$

where  $z = (t - a)/b$ .

According to this equation, if  $\frac{C_o - C}{C_o}$  is plotted as a function of time on normal probability paper, the points should lie on a straight line. Kidnay (1968, p. 106) shows some results of such a plot, which are excellent. This method correlates the data very well, but since the coefficients a and b are empirical their extrapolation would be uncertain.

Theory of Similarity Method: Nemeth (1963, p. 6)

employed the theory of similarity in his treatment. An equation was developed, for the section of the breakthrough curve up to the breakpoint, in the case of the adsorption of solvent vapors by granulated active charcoal. This work, however, is very confusing and difficult to understand.

## DIMENSIONAL ANALYSIS

The scope as well as the limitations of dimensional analysis have been summarized by Langhaar (1951, p. 1) who states:

Dimensional analysis is a method by which we deduce information about a phenomenon from a single premise that the phenomenon can be described by a dimensionally correct equation among certain variables. The generality of the method is both its strength and its weakness. With little effort, a partial solution to nearly any problem is obtained. On the other hand, a complete solution is not obtained nor is the inner mechanism of a phenomenon revealed by dimensional reasoning alone.

Dimensional analysis differs from other methods of approach in that it does not yield equations which can be solved. It does, however, combine the variables into dimensionless groups which facilitate the interpretation and extend the range of application of experimental data. In heat transfer, for example, the convective heat-transfer coefficients are generally calculated from empirical equations obtained by correlating experimental data with the aid of dimensional analysis.

The most serious limitation of dimensional analysis is that it gives no information about the nature of the phenomenon. In fact, to apply dimensional analysis it is necessary to know beforehand what variables influence the phenomenon, and the success or the failure of the method

depends on the proper selection of these variables. It is therefore necessary to have at least a preliminary theory or a thorough physical understanding of a phenomenon before a dimensional analysis can be performed.

The steps in a dimensional analysis may be summarized as follows:

- 1) Write out the proposed relation.
- 2) Determine the number of dimensionless groups. This is equal to the number of variables minus the number of fundamental dimensions.
- 3) Select the primary quantities. The criteria for selection are:
  - (i) Among them, the primary quantities contain all of the dimensions.
  - (ii) The number of primary quantities is equal to the number of variables minus the number of independent dimensionless groups.

Selection of primary quantities is arbitrary; varying the selection will alter the dimensionless groups obtained, but the results will be equivalent.

- 4) Form the dimensionless groups by adding, in turn, each of the remaining variables to the primary quantities.

Many detailed dimensional analyses are given in the heat-transfer texts. McAdams (1942, p. 89), for example,

analyzes the forced-convection heat-transfer in circular tubes.

## THE CORRELATION

The experimental data used in the correlation are for the following systems:

- 1) Methane-Hydrogen on activated charcoal at 76°K
- 2) Nitrogen-Hydrogen on activated charcoal at 76°K
- 3) Methane-Helium on activated charcoal at 76°K
- 4) Nitrogen-Helium on activated charcoal at 76°K
- 5) Methane-Hydrogen on synthetic zeolite at 76°K
- 6) Nitrogen-Hydrogen on synthetic zeolite at 76°K

The first two systems are taken from the Ph.D. thesis of A. J. Kidnay (1968), the third and fourth systems from Kidnay and Hiza (1970), and the last two systems from Kidnay and Hiza (1966).

The breakthrough curves for the charcoal systems are shown in Figures 3 to 10. The synthetic zeolite systems were considered in the final step in the correlation, as will be seen.

#### Step-Function Breakthrough

In fixed-bed adsorption two mass transfer processes take place: the diffusion through the gas phase, and diffusion into the solid particle. If both of these processes were instantaneous, a plot of the adsorber outlet concentration versus time would be a step function.

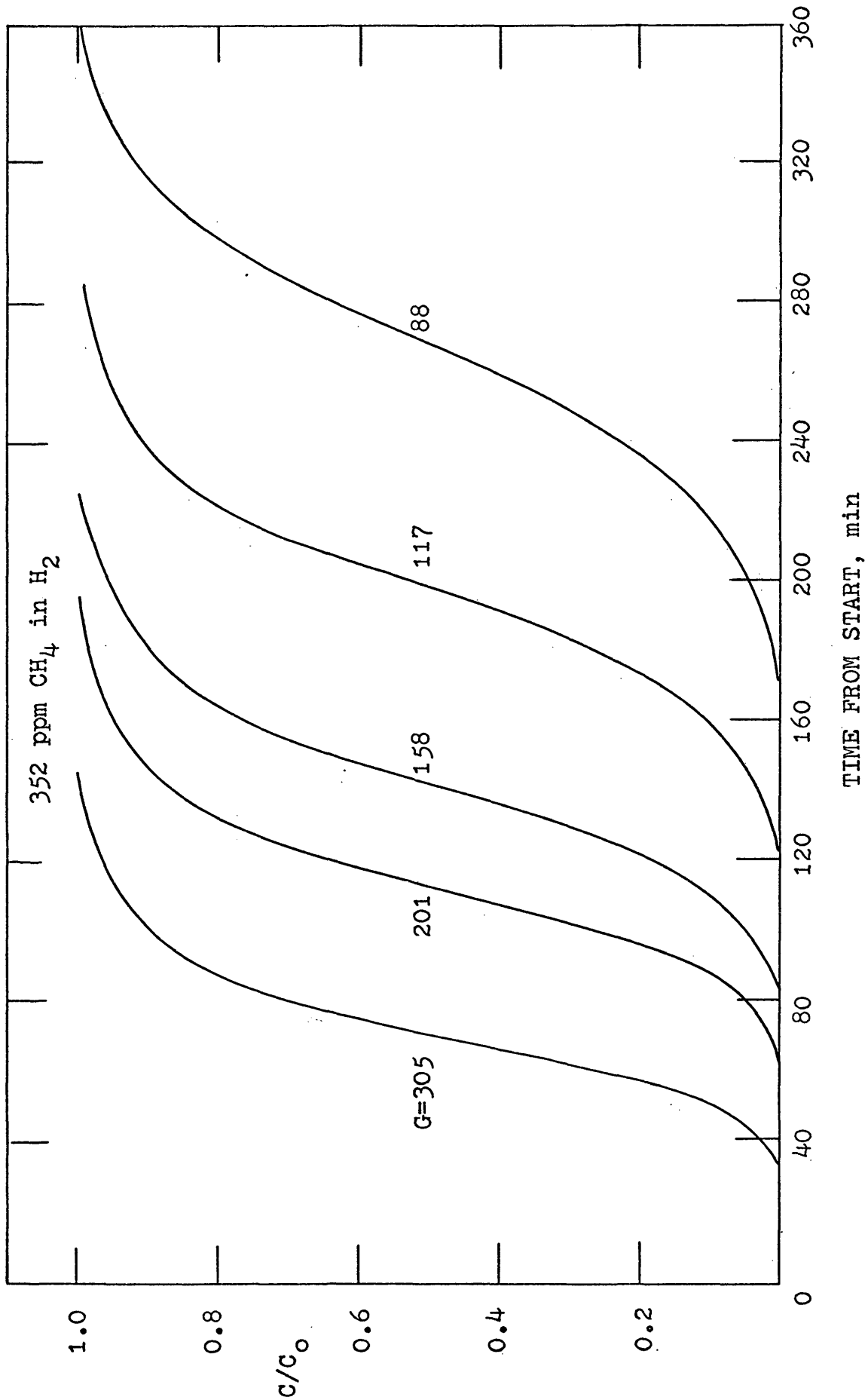


Figure 3. Breakthrough Curves For Methane-Hydrogen On Charcoal

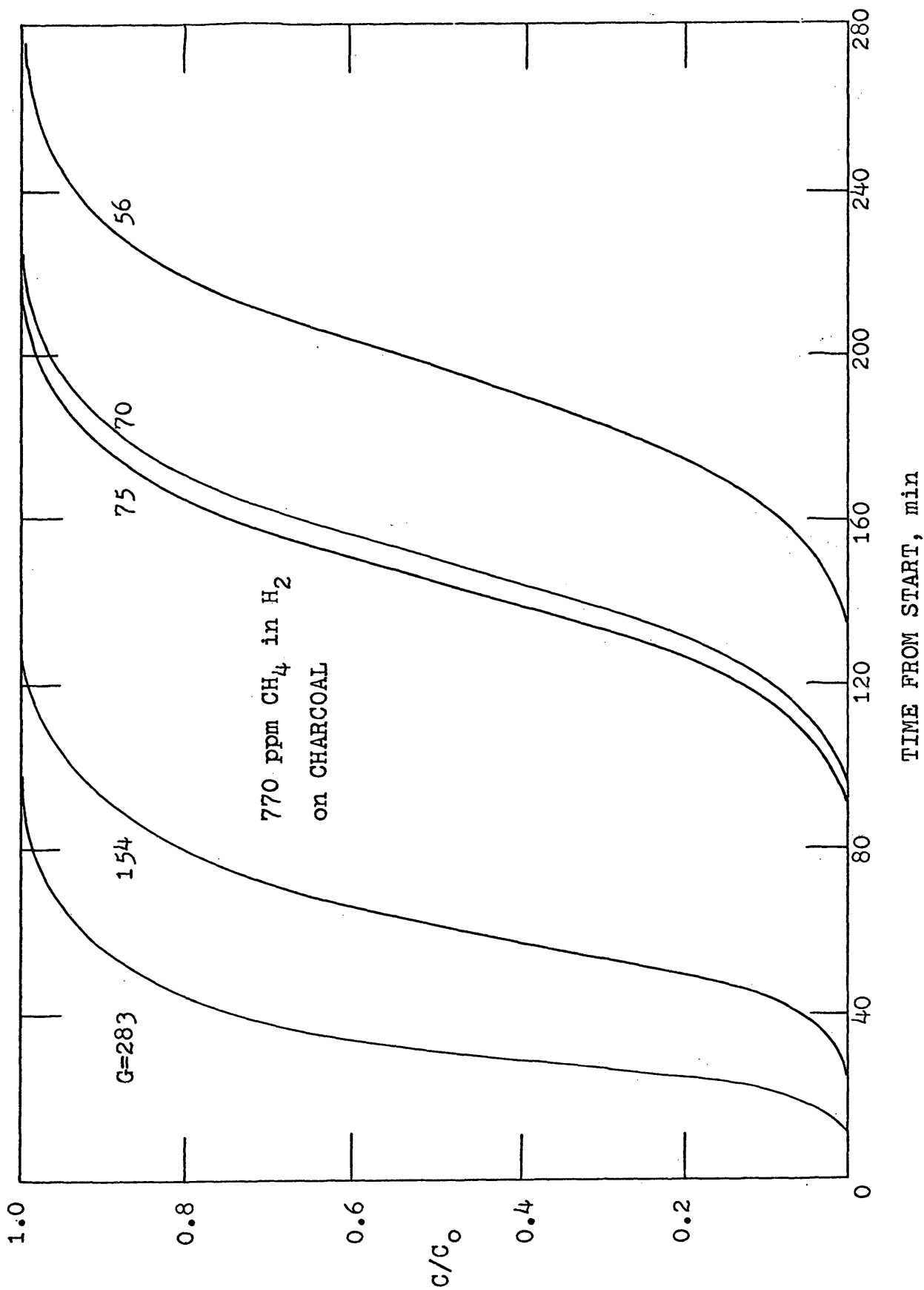


Figure 4. Breakthrough Curves For Methane-Hydrogen On Charcoal

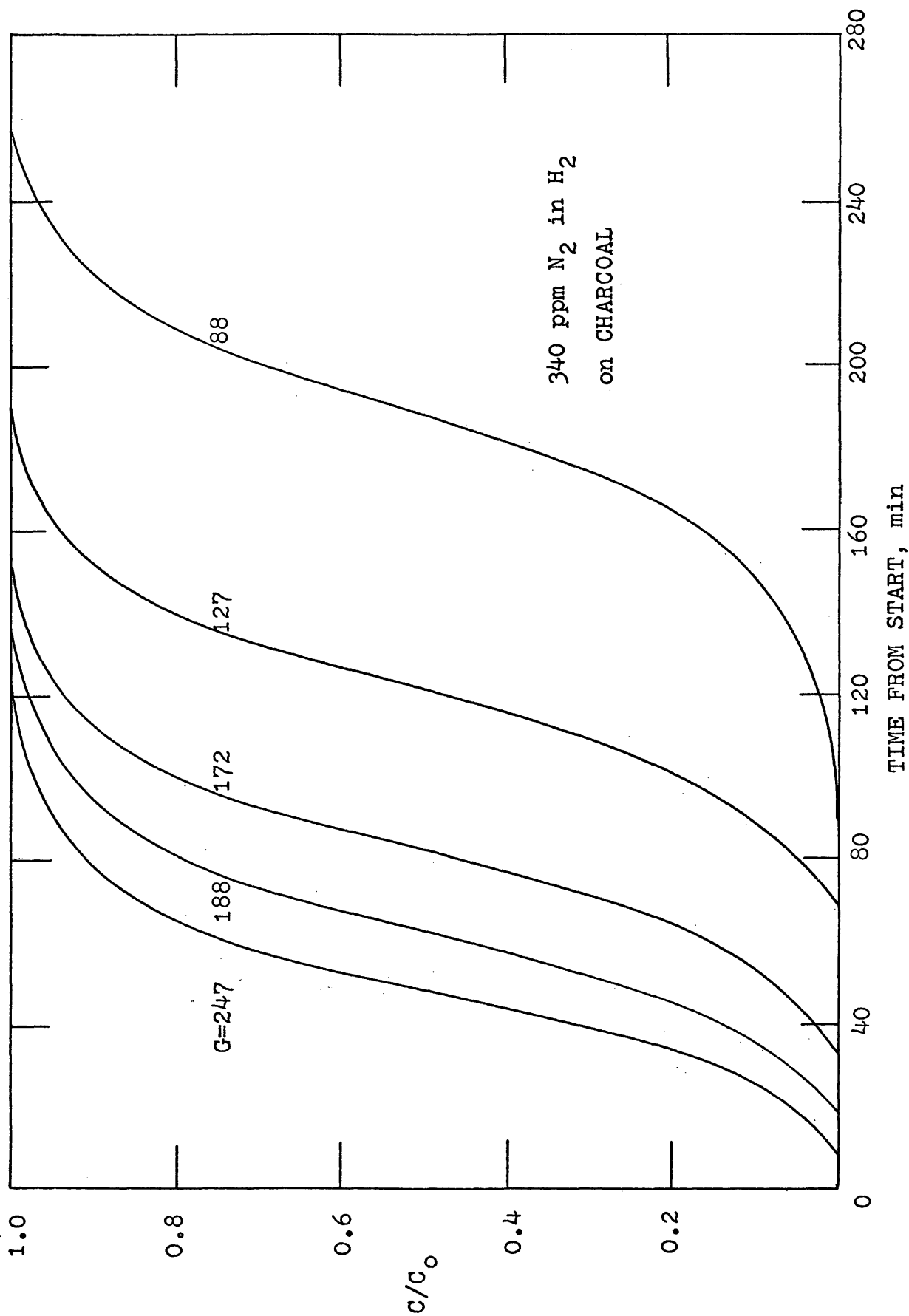


Figure 5. Breakthrough Curves For Nitrogen-Hydrogen On Charcoal

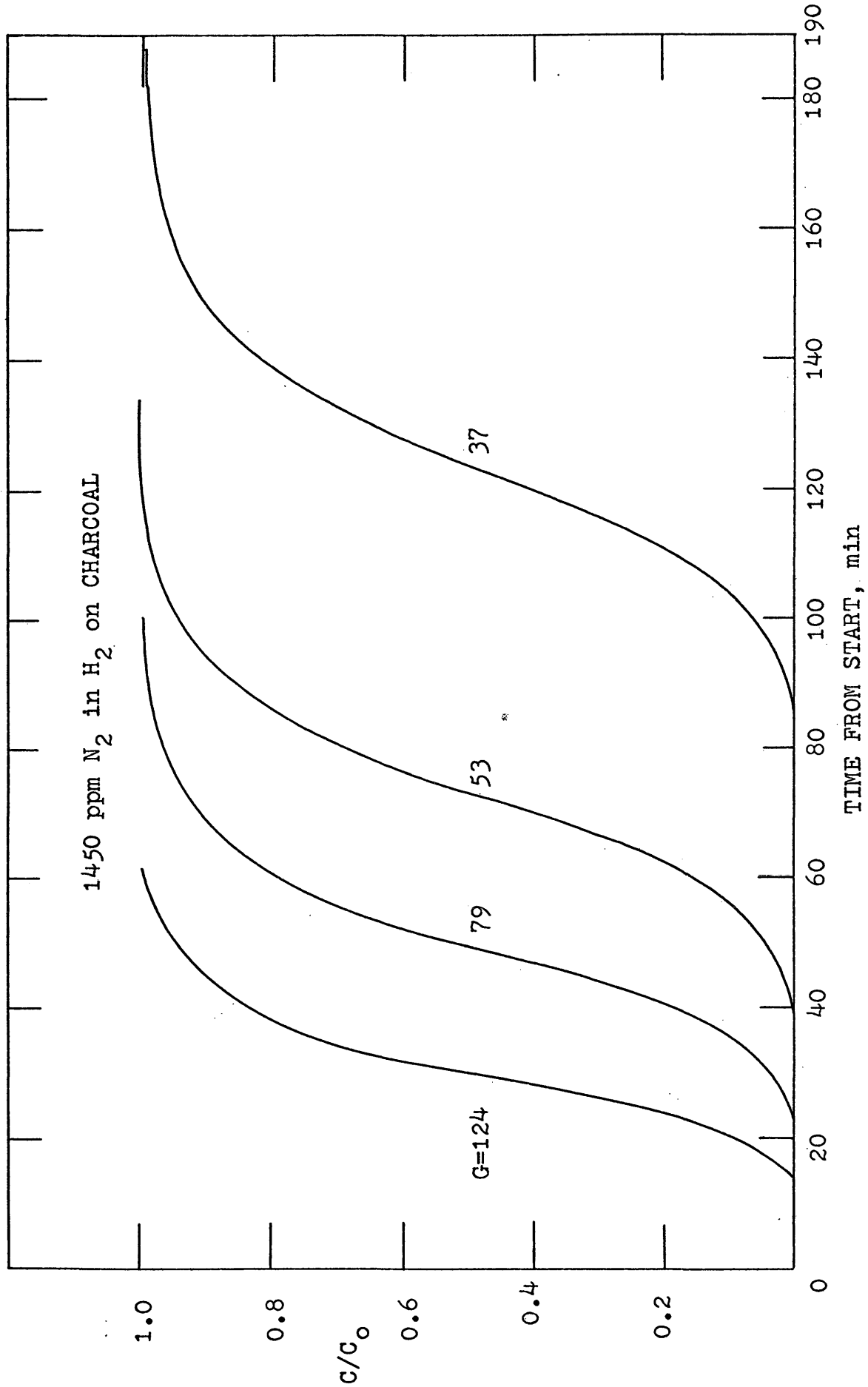


Figure 6. Breakthrough Curves For Nitrogen-Hydrogen On Charcoal

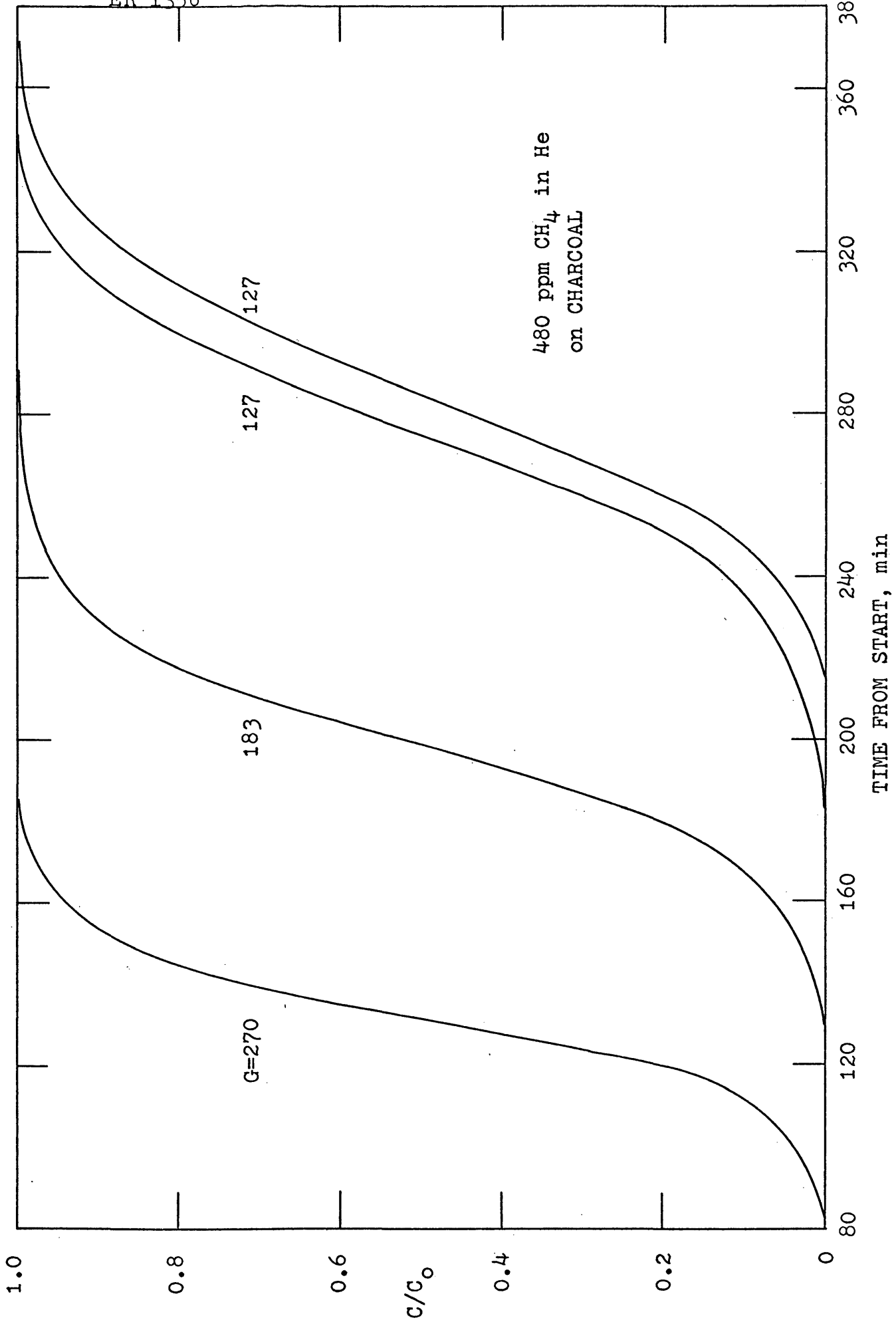


Figure 7. Breakthrough Curves For Methane-Helium On Charcoal

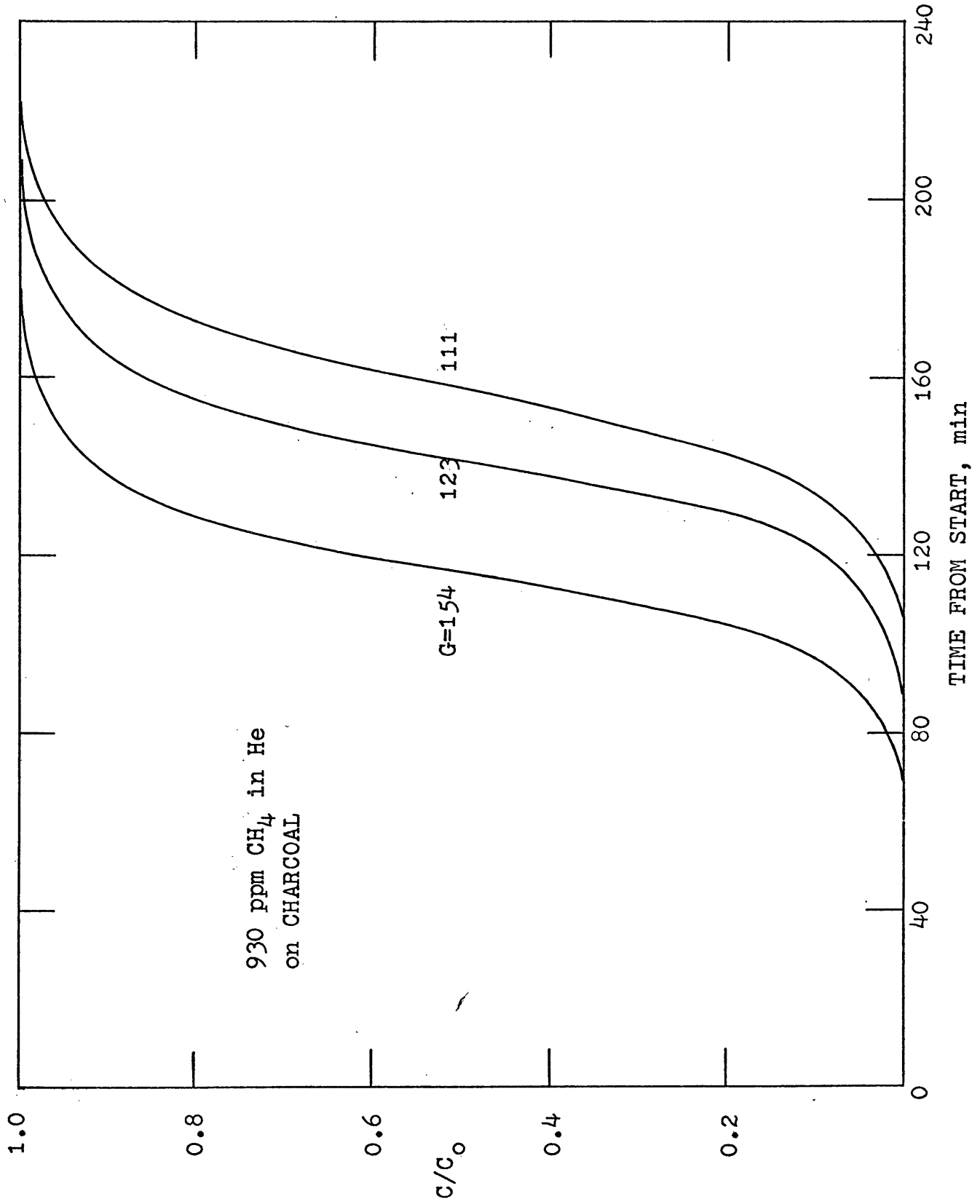


Figure 8. Breakthrough Curves For Methane-Helium On Charcoal

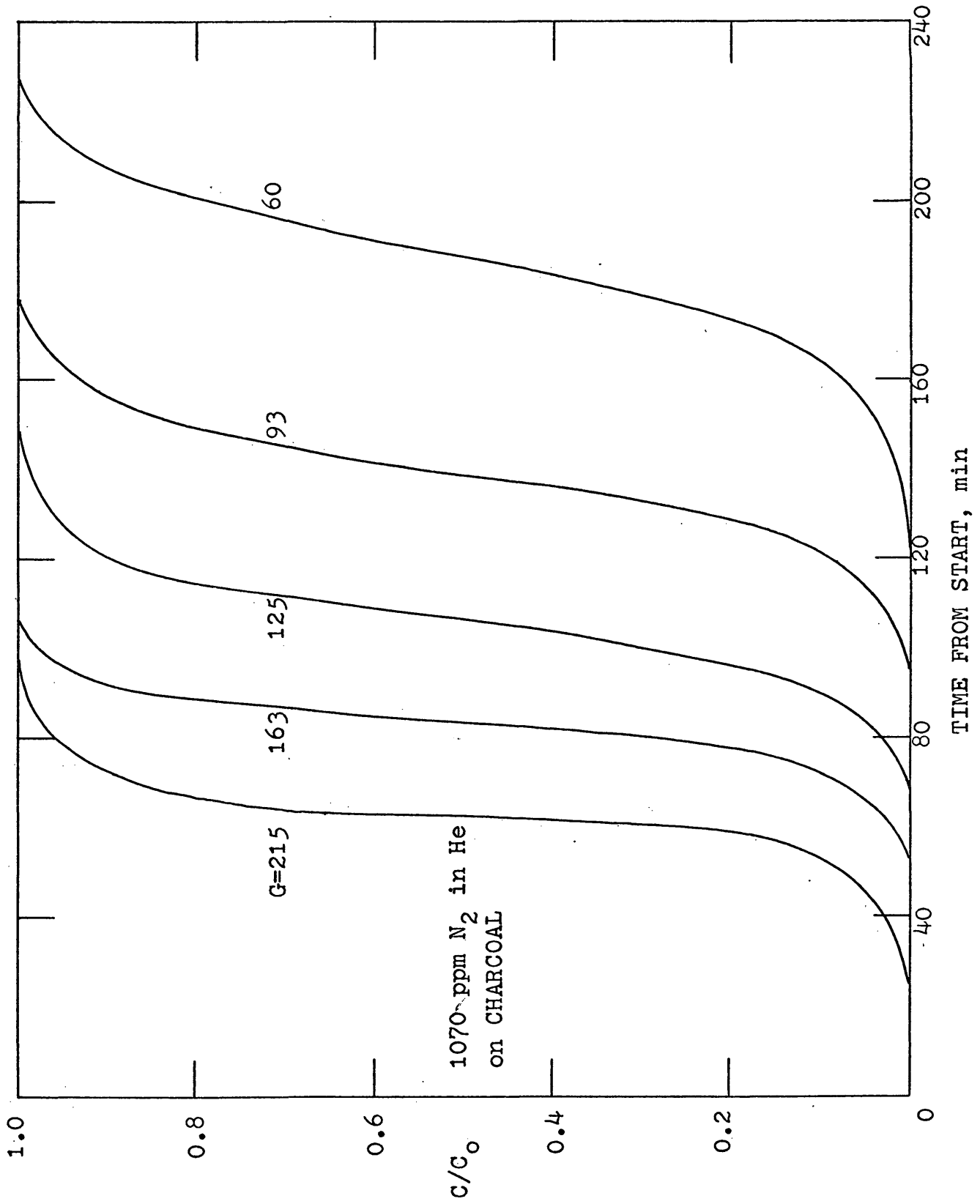


Figure 9. Breakthrough Curves For Nitrogen-Helium On Charcoal

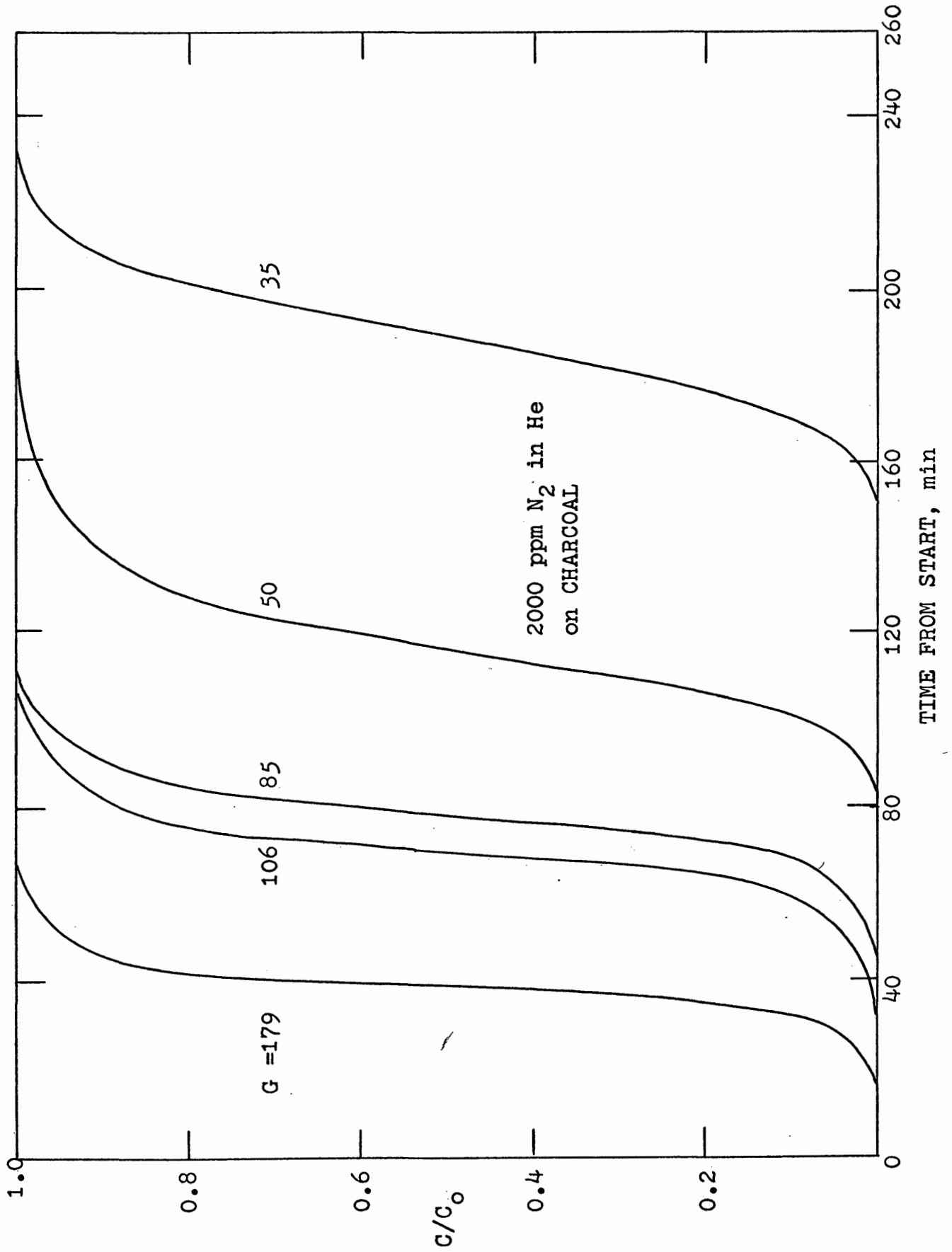
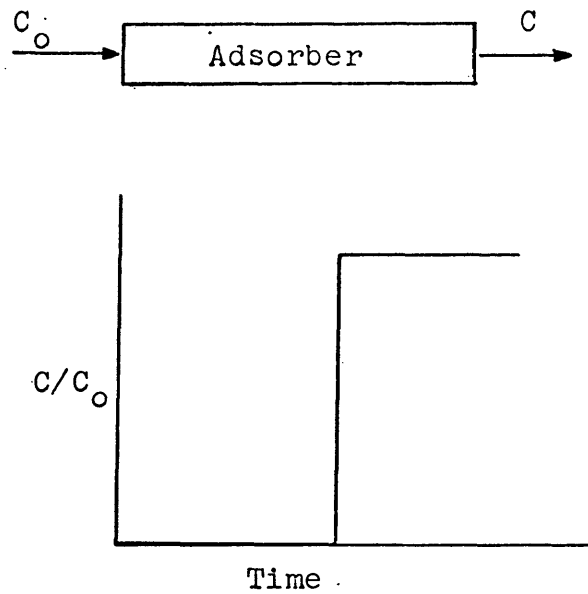
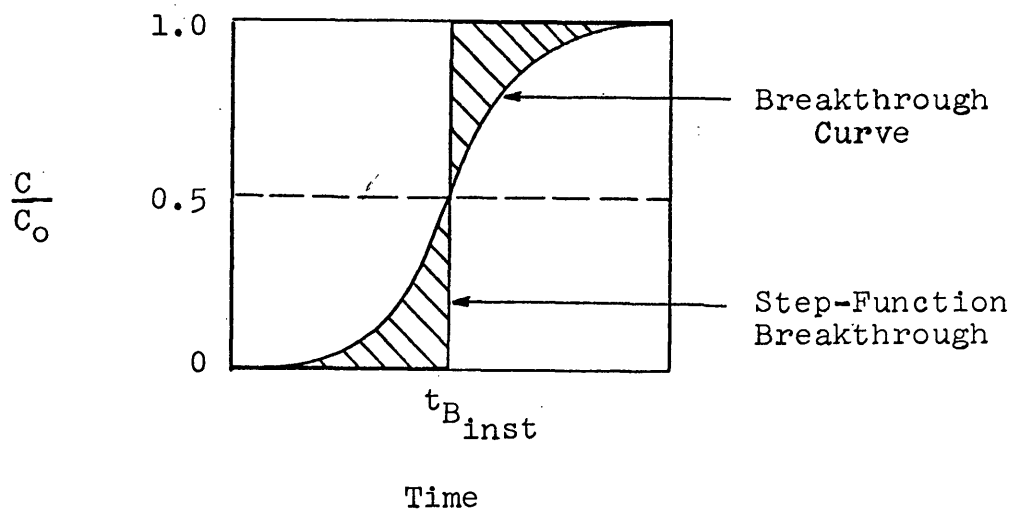


Figure 10. Breakthrough Curves for Nitrogen-Helium on Charcoal



Usually, however, one or both transfer processes are relatively slow, with the result that the breakthrough curve assumes an S shape.

If we assume that the breakthrough curve is symmetrical, then the time to the step-function breakthrough would be the time corresponding to  $C/C_0 = 0.5$ , as shown below:



For step-function breakthrough there is no resistance to mass transfer. Therefore, by making a mass balance, the capacity of the bed (expressed as lb adsorbate/lb solid) is given by the equation:

$$v = \frac{GC_0 t_{B_{inst}}}{m}$$

where  $G$  is the mass flow rate,  $C_0$  is the inlet gas concentration expressed in mass fraction,  $t_{B_{inst}}$  is the time to step-function breakthrough as shown above, and  $m$  is the weight of adsorbent in the bed.

The hydrogen and helium runs on charcoal were made using the same adsorber bed. The breakthrough curves for these systems are shown in Figures 3 to 10. It is seen that these curves are symmetrical, so the time to  $C/C_0 = 0.5$  is taken as the step-function breakthrough time.

Since  $m$  is constant for all the runs, a plot of  $\frac{t_{B_{inst}} C_0}{v}$  versus  $G$  should be a straight line. Or if plotted on a log-log paper, it should be a straight line with a slope of -1. Figure 11 shows such a plot for the hydrogen and helium systems on charcoal. (Note: the  $G$  used in the calculation is in lb/hr-ft<sup>2</sup>. This is all right since the bed cross-sectional area is the same for the systems considered.)

Figure 11 shows some scattering of points. This is due to either experimental error or unsymmetrical breakthrough curves. Experimental error is suspected to be the cause of the scattering because the breakthrough curves considered are exceptionally symmetrical.

Table 1  
Step-Function Breakthrough Correlation  
for the Charcoal System

System	C <sub>O</sub> Mole Fraction	Mass Fraction	t <sub>Binst</sub> min	G lb/hr-ft <sup>2</sup>	v lb impurity lb solid	$\frac{t_{Binst} C_o}{v}$
CH <sub>4</sub> in H <sub>2</sub>	0.00077	0.00616	31	283	0.155	1.23
"	"	"	63	153	0.155	2.50
"	"	"	145	75	0.166	5.38
"	"	"	150	70	0.164	5.63
"	"	"	197	56	0.170	7.14
"	0.000352	0.00282	70	305	0.155	1.27
"	"	"	113	201	0.158	2.01
"	"	"	142	158	0.157	2.55
"	"	"	197	117	0.163	3.41
"	"	"	268	88	0.162	4.67

Table 1  
(Continued)

System	$C_o$ Mole Fraction	Mass Fraction	$t_{Binst}$ min	G lb/hr-ft <sup>2</sup>	$v$ lb impurity lb solid	$\frac{t_{Binst} C_o}{v}$
N <sub>2</sub> in H <sub>2</sub>	0.00145	0.0203	31	124	0.231	2.72
"	"	"	33	119	0.225	3.00
"	"	"	50	79	0.235	4.32
"	"	"	74	53	0.243	6.18
"	"	"	124	37	0.250	10.07
"	0.00034	0.00476	50	247	0.160	1.49
"	"	"	64	188	0.151	2.02
"	"	"	83	172	0.175	2.26
"	"	"	122	127	0.187	3.11
"	"	"	187	89	0.201	4.43

Table 1  
(Continued)

System	Mole Fraction	C <sub>o</sub> Mass Fraction	t <sub>B inst</sub> min	G lb/hr-ft <sup>2</sup>	v $\frac{\text{lb impurity}}{\text{lb solid}}$	$\frac{t_{B \text{ inst } C_o}}{v}$
CH <sub>4</sub> in He	0.00093	0.00372	115	154	0.173	2.47
"	"	"	157	111	0.162	3.61
"	"	"	142	123	0.170	3.11
"	0.00048	0.00192	284	127	0.168	3.25
"	"	"	198	183	0.172	2.21
"	"	"	131	270	0.167	1.51
"	"	"	275	127	0.161	3.28
N <sub>2</sub> in He	0.002	0.014	40	179	0.283	1.98
"	"	"	70	106	0.272	3.60
"	"	"	79	85	0.282	3.92
"	"	"	117	50	0.268	6.11
"	"	"	189	35	0.246	10.76

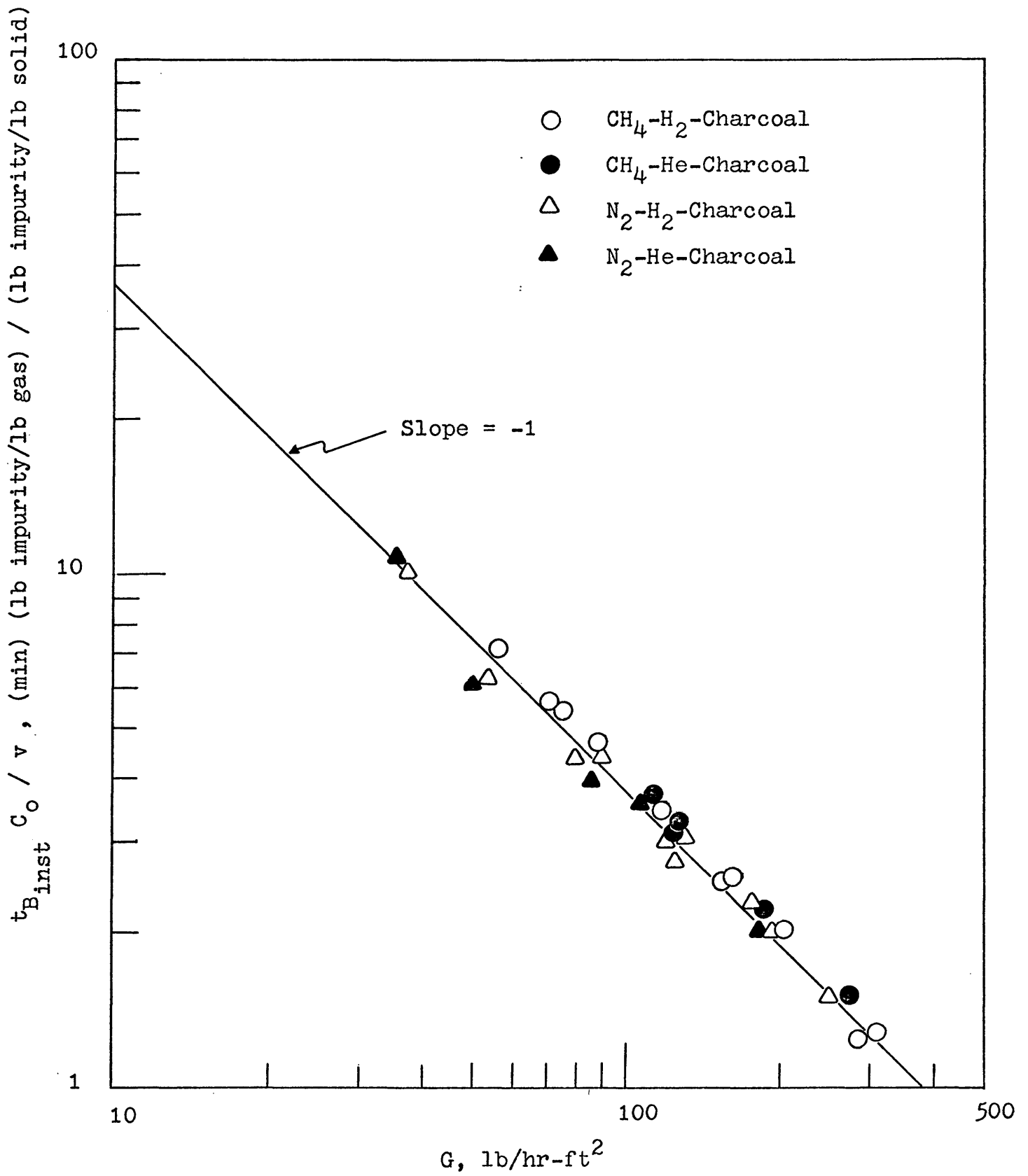


Figure 11. Step-Function Breakthrough Correlation For Charcoal Systems

### The Breaktime

The step-function breakthrough time was shown to be a function of  $G$ , the mass velocity of the gas,  $C_0$  the gas initial concentration,  $v$  the bed capacity, and  $m$  the weight of the adsorbent in the bed.

$$m = \rho_B Q$$

where  $\rho_B$  is the bulk density of the bed, and  $Q$  is the bed volume.

$$G = \rho V$$

where  $\rho$  is the gas density, and  $V$  the gas velocity. Replacing  $m$  and  $G$  in the relationship for the step-function breakthrough, we obtain the following

$$\begin{aligned} t_{B_{inst}} &= f(C_0, V, v, \rho, \rho_B, Q) \\ &= \frac{v \rho_B Q}{\rho V C_0} \end{aligned}$$

The breakpoint is arbitrarily chosen to correspond to  $C/C_0 = 0.1$ .

To correlate the breaktime, two correction factors must be introduced to take into account the resistances to mass transfer in the gas phase and diffusion into the solid particle. These are: (1)  $k_g$ , the mass transfer coefficient in the gas phase, and (2)  $k_s$ , the "solid film" mass transfer coefficient.

Not much is known about  $k_s$ . Too few data are available to provide a reliable basis for its prediction, the

difficulty stemming largely from the lack of ways to describe the complicated pore geometry.

Kidnay (1968, p. 102) found that for the methane-hydrogen and nitrogen-hydrogen systems on charcoal,  $k_s$  is independent of the mass flow rate and the total pressure, and that although the data show considerable scatter,  $k_s$  is a function of  $C_0$ . It is not possible to determine from the data of Eagleton and Bliss (1953, p. 547) if there is a concentration dependence of  $k_s$ . When the  $k_s$  values of Nutter and Burnet (1966, p. 2) are examined, however, it becomes apparent that over a very wide range of inlet concentrations,  $k_s$  is a linear function of  $C_0$ . Thus it seems reasonable to assume that a linear relation will also correlate the  $k_s$  values for the methane-hydrogen and nitrogen-hydrogen on charcoal systems. Therefore,  $k_s$  will be considered in the analysis through  $C_0$ .

The gas phase mass transfer coefficient  $k_g$  is correlated by the following relation

$$\frac{k_g D_p}{D_v} = f(\text{Re}, \text{Sc})$$

where  $D_p$  is the particle diameter, and  $D_v$  the diffusion coefficient. The dimensionless Reynolds and Schmidt numbers are defined by

$$\text{Re} = \frac{D_p G}{\mu}$$

$$\text{Sc} = \frac{\mu}{\rho D_v}$$

where  $\mu$  and  $\rho$  are the viscosity and density of the fluid, and  $G$  is the mass velocity of the fluid.

From above it is seen that

$$k_g = f(D_p, D_v, \rho, \mu)$$

Introducing this to the relationship obtained for step-function breakthrough time, the actual breaktime  $t_B$  will, therefore, be a function of the following variables:

$$t_B = f(C_o, V, v, \rho, \mu, D_p, D_v, \rho_B, Q)$$

Dimensional Analysis: Table 2 lists the variables influencing the breaktime with associated symbols, dimensions, and units.

The number of dimensionless groups is equal to the number of variables minus the number of fundamental dimensions. There are 10 variables and 3 (M, L,  $\theta$ ) dimensions, so there will be 7 dimensionless groups.

The primary quantities selected are:  $\rho$ ,  $D_p$ , and  $\mu$ . Note that among them, the 3 primary variables contain all of the dimensions.

Thus:

$$\pi_1 = t_B \rho^a D_p^b \mu^c = (\theta) \left(\frac{M}{L^3}\right)^a (L)^b \left(\frac{M}{L\theta}\right)^c$$

$$\Sigma M = 0 \quad : \quad a + c = 0$$

$$\Sigma L = 0 \quad : \quad -3a + b - c = 0$$

$$\Sigma \theta = 0 \quad : \quad 1 - c = 0$$

$$a = -1, \quad b = -2, \quad c = 1$$

Table 2  
The Variables Influencing Adsorption

Quantity	Symbol	Dimensions (ML $\theta$ T system)	Units in the Engineering System
Initial gas concentration	$C_0$	dimensionless	$\frac{\text{lb adsorbate}}{\text{lb gas}}$
Gas velocity	$V$	$L/\theta$	ft/sec
Bed capacity	$v$	dimensionless	$\frac{\text{lb adsorbate}}{\text{lb solid}}$
Gas density	$\rho$	$M/L^3$	lb/ft <sup>3</sup>
Bulk density of bed	$\rho_B$	$M/L^3$	$\frac{\text{lb solid}}{\text{ft}^3 \text{ of bed}}$
Bed volume	$Q$	$L^3$	ft <sup>3</sup>
Gas viscosity	$\mu$	$M/L\theta$	lb/ft-sec
Particle diameter	$D_p$	$L$	ft
Diffusion coefficient	$D_v$	$L^2/\theta$	ft <sup>2</sup> /sec
Breaktime	$t_B$	$\theta$	sec

$$\pi_1 = \frac{t_B \mu}{\rho D_p^2}$$

$$\pi_2 = C_o \rho^a D_p^b \mu^c = (-) \left(\frac{M}{L^3}\right)^a (L)^b \left(\frac{M}{L\theta}\right)^c$$

$$\Sigma M = 0 : a + c = 0$$

$$\Sigma L = 0 : -3a + b - c = 0$$

$$\Sigma \theta = 0 : -c = 0$$

$$a = 0, b = 0, c = 0$$

$$\pi_2 = C_o$$

$$\pi_3 = V \rho^a D_p^b \mu^c = \left(\frac{L}{\theta}\right) \left(\frac{M}{L^3}\right)^a (L)^b \left(\frac{M}{L\theta}\right)^c$$

$$\Sigma M = 0 : a + c = 0$$

$$\Sigma L = 0 : 1 - 3a + b - c = 0$$

$$\Sigma \theta = 0 : -1 - c = 0$$

$$a = 1, b = 1, c = -1$$

$$\pi_3 = \frac{V \rho D_p}{\mu}$$

$$\pi_4 = v \rho^a D_p^b \mu^c = (-) \left(\frac{M}{L^3}\right)^a (L)^b \left(\frac{M}{L\theta}\right)^c$$

$$\Sigma M = 0 : a + c = 0$$

$$\Sigma L = 0 : -3a + b - c = 0$$

$$\Sigma \theta = 0 : -c = 0$$

$$a = 0, b = 0, c = 0$$

$$\pi_4 = v$$

$$\pi_5 = D_v \rho^a D_p^b \mu^c = \left(\frac{L^2}{\theta}\right) \left(\frac{M}{L^3}\right)^a (L)^b \left(\frac{M}{L\theta}\right)^c$$

$$\Sigma M = 0 : a + c = 0$$

$$\Sigma L = 0 : 2 - 3a + b - c = 0$$

$$\Sigma \theta = 0 : -1 - c = 0$$

$$a = 1, b = 0, c = -1$$

$$\pi_5 = \frac{D_v \rho}{\mu}$$

$$\pi_6 = \rho_B \rho^a D_p^b \mu^c = \left(\frac{M}{L^3}\right) \left(\frac{M}{L^3}\right)^a (L)^b \left(\frac{M}{L\theta}\right)^c$$

$$\Sigma M = 0 : 1 + a + c = 0$$

$$\Sigma L = 0 : -3 - 3a + b - c = 0$$

$$\Sigma \theta = 0 : -c = 0$$

$$a = -1, b = 0, c = 0$$

$$\pi_6 = \frac{\rho_B}{\rho}$$

$$\pi_7 = Q \rho^a D_p^b \mu^c = (L^3) \left(\frac{M}{L^3}\right)^a (L)^b \left(\frac{M}{L\theta}\right)^c$$

$$\Sigma M = 0 : a + c = 0$$

$$\Sigma L = 0 : 3 - 3a + b - c = 0$$

$$\Sigma \theta = 0 : -c = 0$$

$$a = 0, b = -3, c = 0$$

$$\pi_7 = \frac{Q}{D_p^3}$$

Thus

$$f(\pi_1, \pi_2, \pi_3, \pi_4, \pi_5, \pi_6, \pi_7) = 0$$

$$f\left(\frac{t_B \mu}{\rho D_p^2}, C_o, \frac{V \rho D_p}{\mu}, v, \frac{D_v \rho}{\mu}, \frac{\rho_B}{\rho}, \frac{Q}{D_p^3}\right) = 0$$

or

$$\frac{t_B \mu}{\rho D_p^2} = f\left(C_o, \frac{V \rho D_p}{\mu}, v, \frac{D_v \rho}{\mu}, \frac{\rho_B}{\rho}, \frac{Q}{D_p^3}\right)$$

The first dimensionless group will be considered a modified Fourier number based on the breaktime.

$$Fo = \frac{t_B \mu}{\rho D_p^2}$$

while the Reynolds and Schmidt numbers are defined by

$$Re = \frac{V \rho D_p}{\mu}$$

$$Sc = \frac{\mu}{D_v \rho}$$

Therefore, the relationship obtained from the dimensional analysis is

$$Fo = f\left(C_o, Re, v, Sc, \frac{\rho_B}{\rho}, \frac{Q}{D_p^3}\right)$$

This is only a partial solution because it shows that  $Fo$  is some function of the 6 dimensionless groups. The exact dependency of  $Fo$  on each of the groups must be determined using experimental data.

The relationship can be written in the following form:

$$Fo = (\text{constant})(C_o)^a (Re)^b (v)^c (Sc)^d \left(\frac{\rho_B}{\rho}\right)^e \left(\frac{Q}{D_p^3}\right)^f$$

The next step is to determine the above exponents.

Exponent of  $C_o$ : The step-function breakthrough time was shown to be inversely proportional to  $C_o$ . Since this was determined by a mass balance on the adsorbate in the gas stream, the dependency will be the same for the breakthrough time. Therefore  $t_B$  is inversely proportional to  $C_o$ .

Since  $\rho$ ,  $\mu$ , and  $D_p$  are all independent of  $C_o$ ,  $Fo$  is proportional to  $C_o^{-1}$ , or

$$(Fo)(C_o) = f(Re, v, Sc, \frac{\rho_B}{\rho}, \frac{Q}{D_p^3})$$

To determine the actual functional relation of  $Fo$  and the other variables, the response of  $Fo$  to changes in each of the variables (while keeping the others constant) must be investigated. This is an extremely difficult task since it is impossible, with the available sets of data, to keep 4 out of the 5 variables constant, because of interdependency. Only  $Q/D_p^3$  can be kept constant. The Reynolds number, bed capacity, Schmidt number, and the  $\rho_B/\rho$  ratio all vary with pressure. Table 3 lists the experimental and calculated variables for the methane-hydrogen and nitrogen-hydrogen on charcoal systems, and Figure 12 shows a plot of the Schmidt number of hydrogen at the operating conditions versus pressure.

Exponent of  $(\rho_B/\rho)$ : This dimensionless ratio was the next to be considered because it is the most difficult variable to keep constant. All the other variables have to be

Table 3  
 Experimental and Calculated Variables  
 for the Methane-Hydrogen and Nitrogen-  
 Hydrogen on Charcoal Systems

Average Temperature = 76.1°K

$D_p = 0.00633$  ft

Concentration of Impurity on the Inlet Hydrogen Stream	Pressure atm	Mass Flow lb/hr-ft <sup>2</sup>	$\frac{D_p G}{\mu}$	Capacity, v $\frac{\text{lb impurity}}{\text{lb solid}}$
770 ppm CH <sub>4</sub>	82.10	283	168	0.155
" " "	53.50	154	103	0.155
" " "	16.70	75	57	0.166
" " "	5.25	56	44	0.169
" " "	30.75	70	52	0.164
352 ppm CH <sub>4</sub>	72.50	305	191	0.155
" " "	55.70	158	107	0.155
" " "	31.55	201	148	0.158
" " "	21.00	88	67	0.162
" " "	8.10	117	91	0.163
" " "	30.65	135	100	0.158
1450 ppm N <sub>2</sub>	9.90	87	67	0.231
" " "	82.50	124	74	0.231
" " "	69.65	119	75	0.225
" " "	50.70	53	37	0.243
" " "	80.55	79	47	0.235
" " "	30.75	37	27	0.250

Table 3  
(Continued)

Concentration of Impurity on the Inlet Hydrogen Stream	Pressure atm	Mass Flow lb/hr-ft <sup>2</sup>	$\frac{D_p G}{\mu}$	Capacity, v $\frac{\text{lb impurity}}{\text{lb solid}}$
340 ppm N <sub>2</sub>	68.05	188	120	0.152
" " "	55.25	247	166	0.160
" " "	35.50	172	125	0.176
" " "	23.05	127	96	0.186
" " "	9.30	89	69	0.201

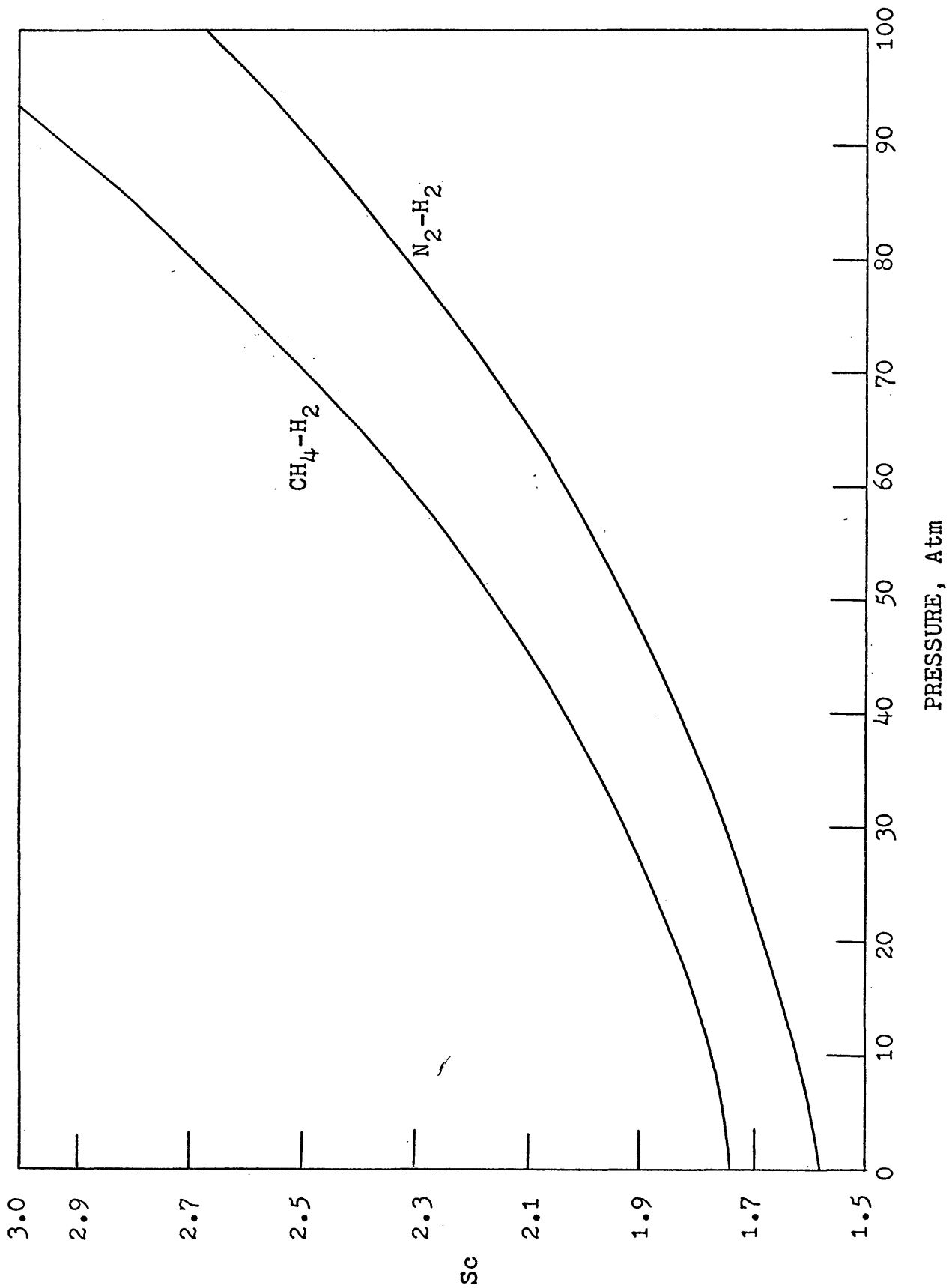


Figure 12. Schmidt Number versus Pressure for  $\text{CH}_4\text{-H}_2$  and  $\text{N}_2\text{-H}_2$

kept constant in order to determine the exponent of  $\rho_B/\rho$ . If  $v$  is to be kept constant, we are limited to the methane-hydrogen system as seen from Table 3. If  $Sc$  is to be kept constant, we are limited to the low pressure region as seen from Figure 12. Since  $Re$  also is to be kept constant, there are only a few data points in the low pressure region of the methane-hydrogen system that can be used. Four data points were chosen and are listed in Table 4. The ratio  $Q/D_p^3$  is constant because the same adsorber and adsorbent are used.

The plot of  $(Fo)(C_0)$  versus  $(\rho_B/\rho)$  is shown in Figure 13. The best line passing through the 4 points has a slope of 1.3, but since  $Re$  and  $Sc$  are not exactly constant, the determination of the exponent of  $\rho_B/\rho$  from Figure 13 is not exact.

Since the step-function breakthrough time was shown to be proportional to  $\rho_B/\rho$ , the same functional relation is assumed for the breaktime, because when the resistance to transfer was considered, the only thing that differed in the analysis was the introduction of  $k_g$  which is usually a function only of  $Re$  and  $Sc$ . A line of slope = 1 is shown in Figure 13. The deviation between the data points and the line of unit slope is not large bearing in mind the fact that  $Re$  and  $Sc$  are not very constant for the 4 points that were considered.

Therefore,  $(Fo)(C_0)$  is proportional to  $(\rho_B/\rho)$

or

Table 4  
 For the Determination of  
 The Exponent of  $(\rho_B/\rho)$

Pressure atm	Re	Sc	$\frac{v}{\text{lb solid}}$	$\frac{C_o}{\text{lb H}_2}$	Fo	(Fo)(C <sub>o</sub> )	$\frac{\rho_B}{\rho}$
8.10	91	1.76	0.163	0.00282	343.6	9.68	193.7
30.65	100	1.95	0.158	0.00282	755.4	2.13	51.27
53.50	103	2.20	0.155	0.00616	149.3	0.92	30.23
55.70	107	2.23	0.155	0.00282	354.3	1.00	29.06

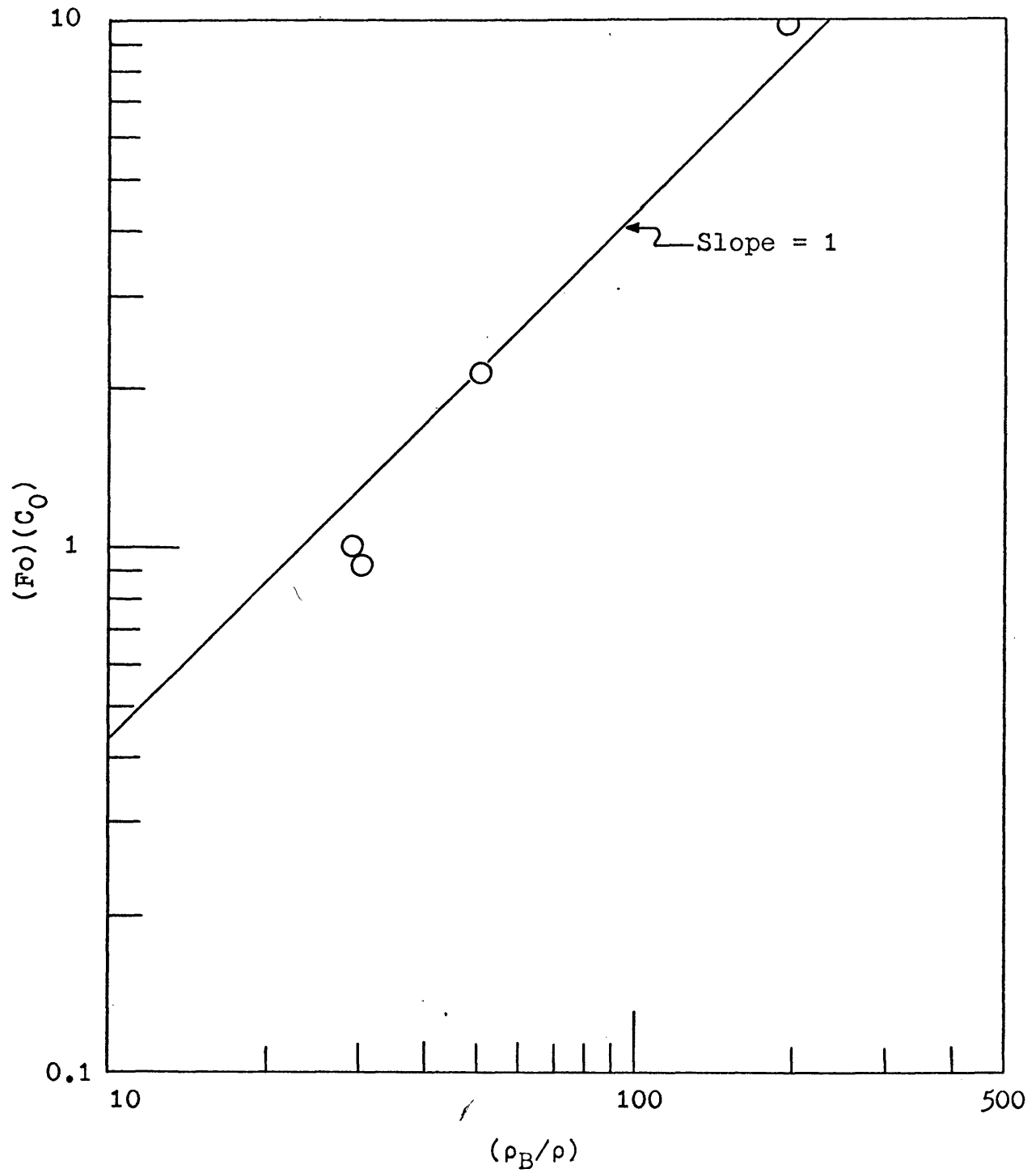


Figure 13. Determination Of The Exponent Of  $(\rho_B/\rho)$

$$\frac{(Fo)(C_o)}{(\rho_B/\rho)} = f(Re, v, Sc, \frac{Q}{D_p^3})$$

Exponent of Re: Seven data points were chosen from the methane-hydrogen system, in the low pressure region, to determine this exponent. Table 5 lists these data points, and shows that  $v$  and  $Sc$  do not vary much. A plot of  $\frac{(Fo)(C_o)}{(\rho_B/\rho)}$  versus  $Re$  is shown in Figure 14. Although the slope of the line is  $-1.09$ , the exponent is taken to be  $-1$ , since this value gave a better final correlation.

Therefore  $\frac{(Fo)(C_o)}{(\rho_B/\rho)}$  is proportional to  $Re^{-1}$

or

$$\frac{(Fo)(C_o)(Re)}{(\rho_B/\rho)} = f(v, Sc, \frac{Q}{D_p^3})$$

Exponent of  $v$ : Table 3 shows that the capacities of the methane-hydrogen system are nearly constant for all the runs, but this is not the case in the nitrogen-hydrogen system. Since  $Sc$  must be kept constant for the determination of the exponent of  $v$ , we are again limited to the low pressure region. Five data points from the nitrogen-hydrogen system, and two from the methane-hydrogen system, were chosen so that  $Sc$  did not vary much, as shown in Table 6. A plot of  $\frac{(Fo)(C_o)(Re)}{(\rho_B/\rho)}$  versus  $v$  is shown in Figure 15. The best line that can be drawn through the points has a slope of  $1.1$ . Since the step-function breakthrough time was

Table 5

For the Determination of the Exponent of Re

Pressure atm	Sc	$\frac{v}{\text{lb solid}}$ lb CH <sub>4</sub>	$\frac{C_o}{\text{lb H}_2}$ lb CH <sub>4</sub>	$\frac{\rho_B}{\rho}$	Fo	$\frac{(Fo)(C_o)}{(\rho_B/\rho)}$	Re
31.55	1.96	0.158	0.00282	49.8	487.4	0.0276	148
21.0	1.86	0.162	0.00282	73.7	1772.0	0.0677	67
8.10	1.76	0.163	0.00282	193.7	3236.0	0.0470	91
30.65	1.95	0.158	0.00282	51.3	755.4	0.0414	100
16.70	1.82	0.166	0.00616	92.1	1168.0	0.0784	57
5.25	1.76	0.169	0.00616	293.8	4939.0	0.104	44
30.75	1.95	0.164	0.00616	50.8	674.6	0.0816	52

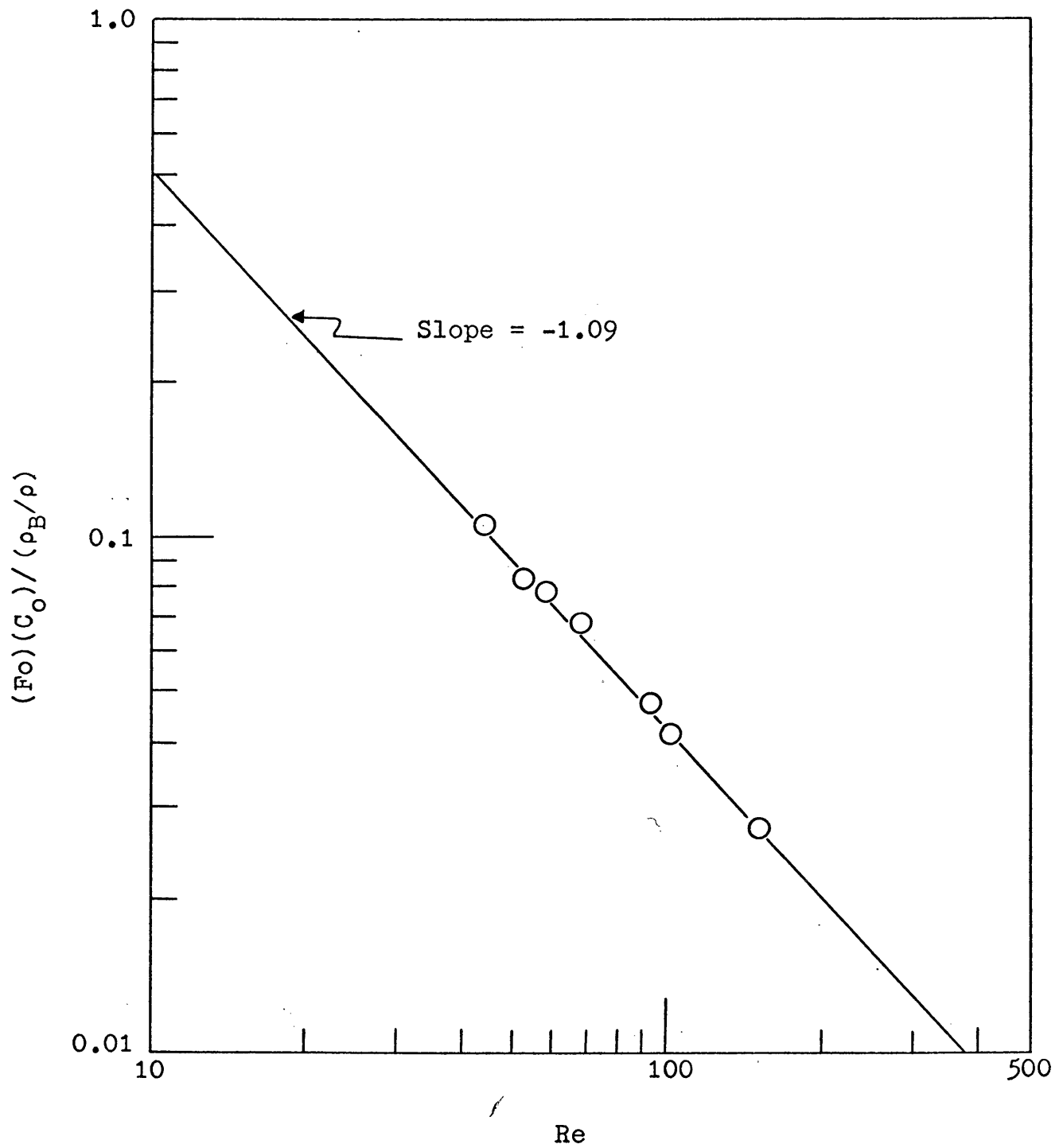


Figure 14. Determination Of The Exponent Of  $Re$

Table 6  
For the Determination of the Exponent of  $v$

System	Pressure atm	Sc	$C_o$ $\frac{\text{lb impurity}}{\text{lb H}_2}$	Re	$\frac{P_B}{p}$	Fo	$\frac{(F_o)(C_o)(Re)}{(P_B/p)}$	$v$ $\frac{\text{lb solid}}{\text{lb impurity}}$
N <sub>2</sub> -H <sub>2</sub> -charcoal	9.3	1.60	0.00476	69	168.7	2598	5.05	0.201
" "	23.05	1.70	0.00476	96	67.9	668	4.49	0.186
" "	35.5	1.80	0.00476	125	43.6	285	3.89	0.176
" "	30.75	1.77	0.0203	27	50.5	575	7.48	0.250
" "	9.9	1.60	0.0203	67	158.5	624	5.36	0.231
CH <sub>4</sub> -H <sub>2</sub> -charcoal	5.25	1.76	0.00616	44	293.8	4939	4.55	0.169
" "	8.10	1.76	0.00282	91	193.7	3236	4.28	0.163

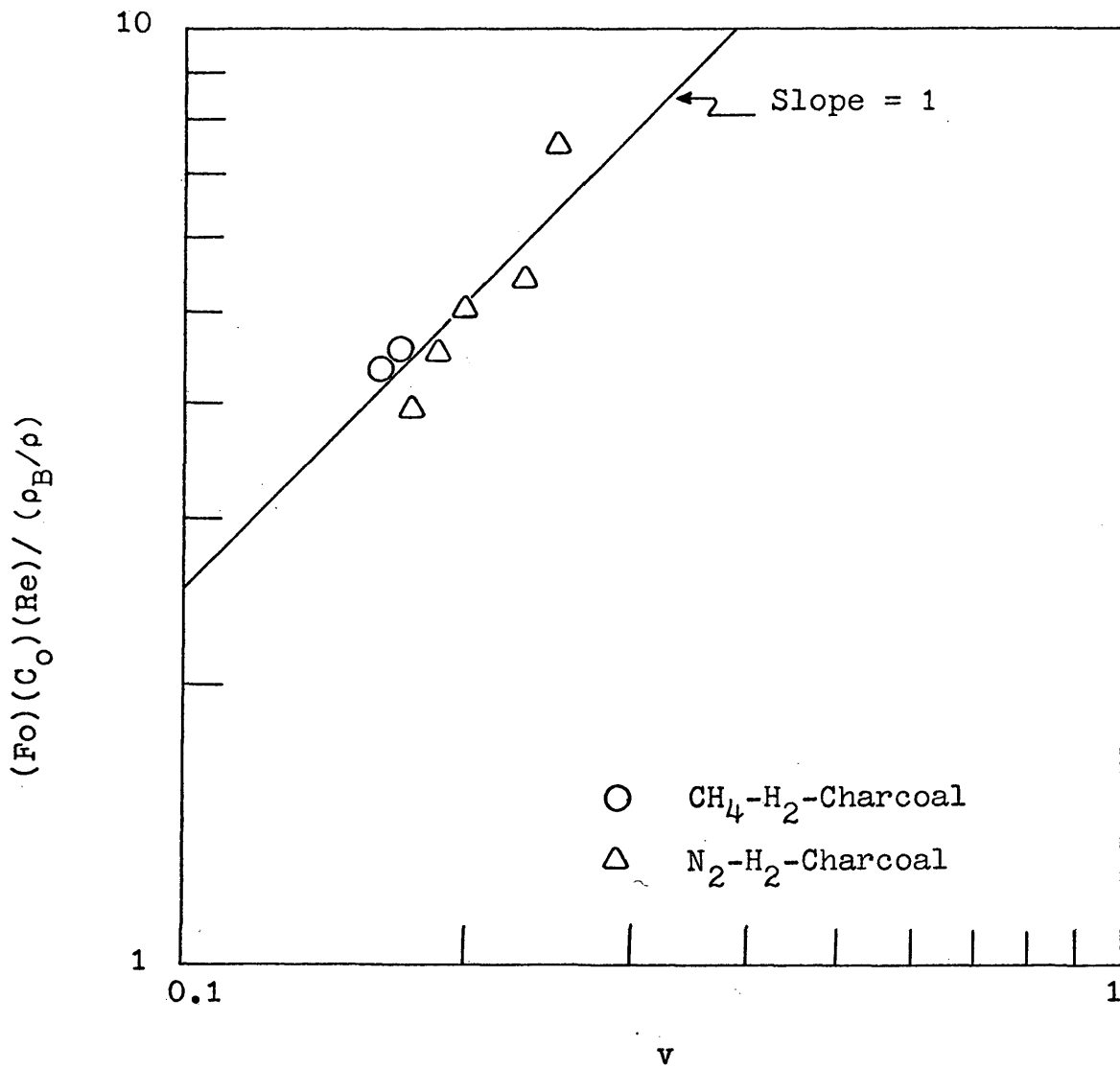


Figure 15. Determination Of The Exponent Of  $v$

shown to be proportional to  $v$ , by the same reasoning used in the determination of the exponent of  $(\rho_B/\rho)$ , the exponent of  $v$  is taken to be 1. A line of slope = 1 is shown in Figure 15.

Therefore  $\frac{(Fo)(C_o)(Re)}{(\rho_B/\rho)}$  is proportional to  $v$

or

$$\frac{(Fo)(C_o)(Re)}{(\rho_B/\rho)(v)} = f(Sc, \frac{Q}{D_p^3})$$

Exponent of Sc: Figure 16 shows a plot of  $\frac{(Fo)(C_o)(Re)}{(\rho_B/\rho)(v)}$  versus  $Sc$  for the methane-hydrogen and nitrogen-hydrogen on charcoal systems. The slope of the line passing through the points is -0.67. There is a difficulty in drawing the line due to the fact that the  $Sc$  values are quite scattered. The determined value of the exponent, however, is reasonable because, as discussed previously, the gas phase mass transfer coefficient is correlated by the following relation

$$\frac{k_g D_p}{D_v} = f(Re, Sc)$$

It has been shown experimentally that  $k_g$  is proportional to  $D_v^{2/3}$  over a wide range of values of  $Sc$ . The above equation reduces to

$$\frac{k_g \rho}{G} Sc^{2/3} = f(Re)$$

The term on the left is called the  $j$  factor for mass transfer,  $j_d$ .

Table 7

For the Determination of the Exponent of Sc

System	$\frac{(Fo)(C_o)(Re)}{(\rho_B/\rho)(v)}$	Sc
CH <sub>4</sub> -H <sub>2</sub> on Charcoal	18.90	2.77
" " "	21.80	2.20
" " "	26.87	1.82
" " "	26.92	1.76
" " "	25.98	1.96
" " "	23.10	2.53
" " "	25.16	2.23
" " "	25.82	1.96
" " "	28.02	1.86
" " "	26.26	1.76
" " "	26.27	1.95
N <sub>2</sub> -H <sub>2</sub> on Charcoal	23.20	1.60
" " "	18.44	2.36
" " "	20.71	2.16
" " "	21.00	1.93
" " "	20.38	2.33
" " "	29.92	1.77
" " "	18.03	2.14
" " "	17.88	1.98
" " "	22.10	1.80
" " "	24.14	1.70
" " "	25.12	1.60

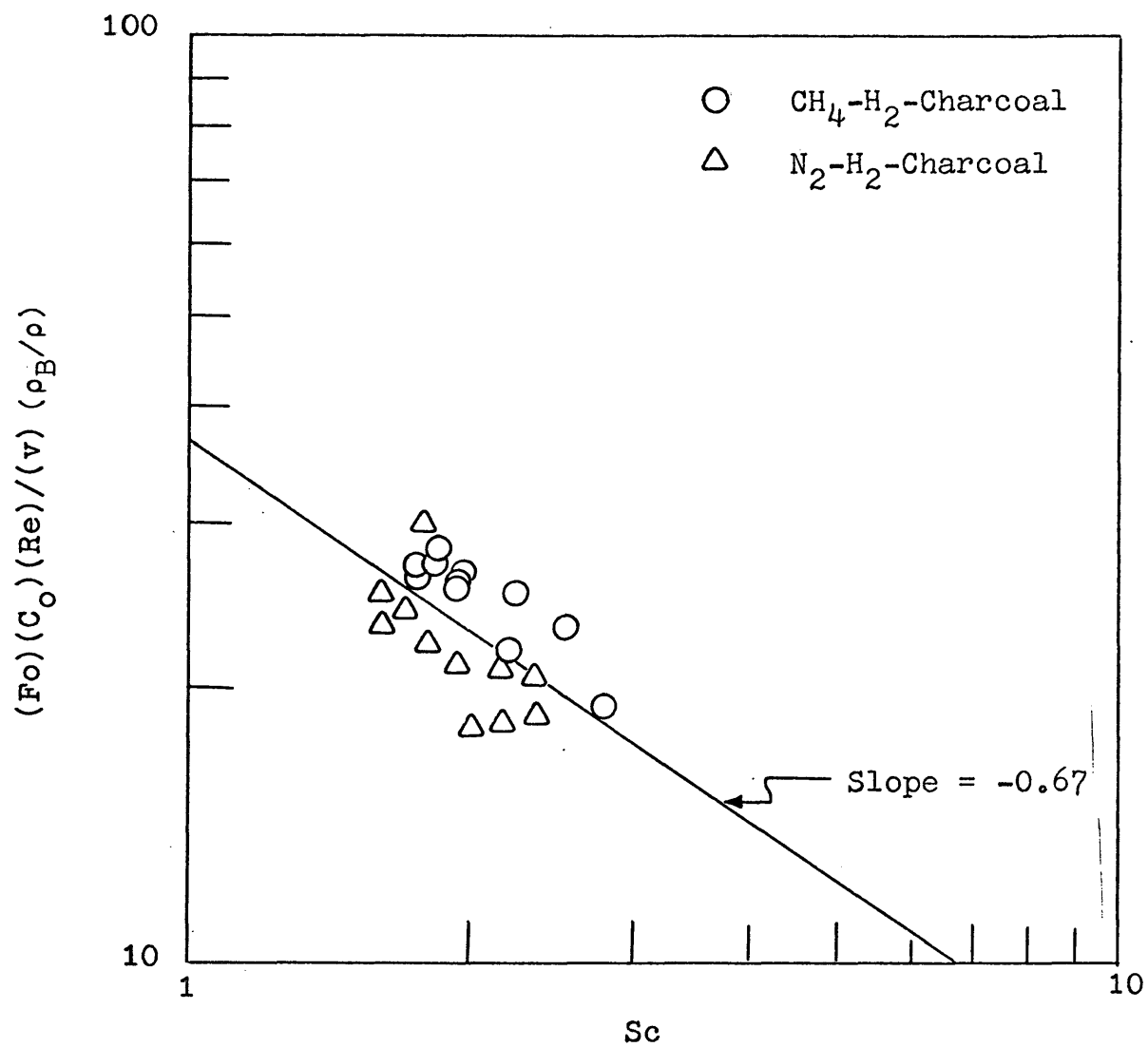


Figure 16. Determination Of The Exponent Of  $Sc$

The above form was suggested by Chilton and Colburn in 1934 as a basis for the correlation of mass-transfer data.

Data on mass transfer to pellets have been summarized by DeAcetis and Thodos by a single curve shown in Figure 17.

Since  $k_g$  is proportional to  $Sc^{-2/3}$ , it is not surprising to find that  $Fo$ , and hence  $t_B$ , is proportional to  $Sc^{-0.67}$ .

Therefore  $\frac{(Fo)(C_o)(Re)}{(\rho_B/\rho)(v)}$  is proportional to  $Sc^{-0.67}$

or

$$\frac{(Fo)(C_o)(Re)(Sc)^{0.67}}{(\rho_B/\rho)(v)} = f\left(\frac{Q}{D_p^3}\right)$$

Exponent of  $Q/D_p^3$ : To determine this exponent more systems are needed. The second system considered is the methane-helium and nitrogen-helium on charcoal at 76°K. These runs were made using the same adsorber and adsorbent, so that  $Q/D_p^3$  is the same as that for the hydrogen runs on charcoal. The third system is the methane-hydrogen and nitrogen-hydrogen on synthetic zeolite at 76°K. The fourth system is the methane-hydrogen on silica gel at -115°F reported by Campbell (1961).

Representative values of  $\frac{(Fo)(C_o)(Re)(Sc)^{0.67}}{(\rho_B/\rho)(v)}$  for each of the above systems are listed in Table 8. Figure 18 shows a plot of  $\frac{(Fo)(C_o)(Re)(Sc)^{0.67}}{(\rho_B/\rho)(v)}$  versus  $Q/D_p^3$ , each system represented by a line to indicate the scatter of points within. The line passing through the "points" has a

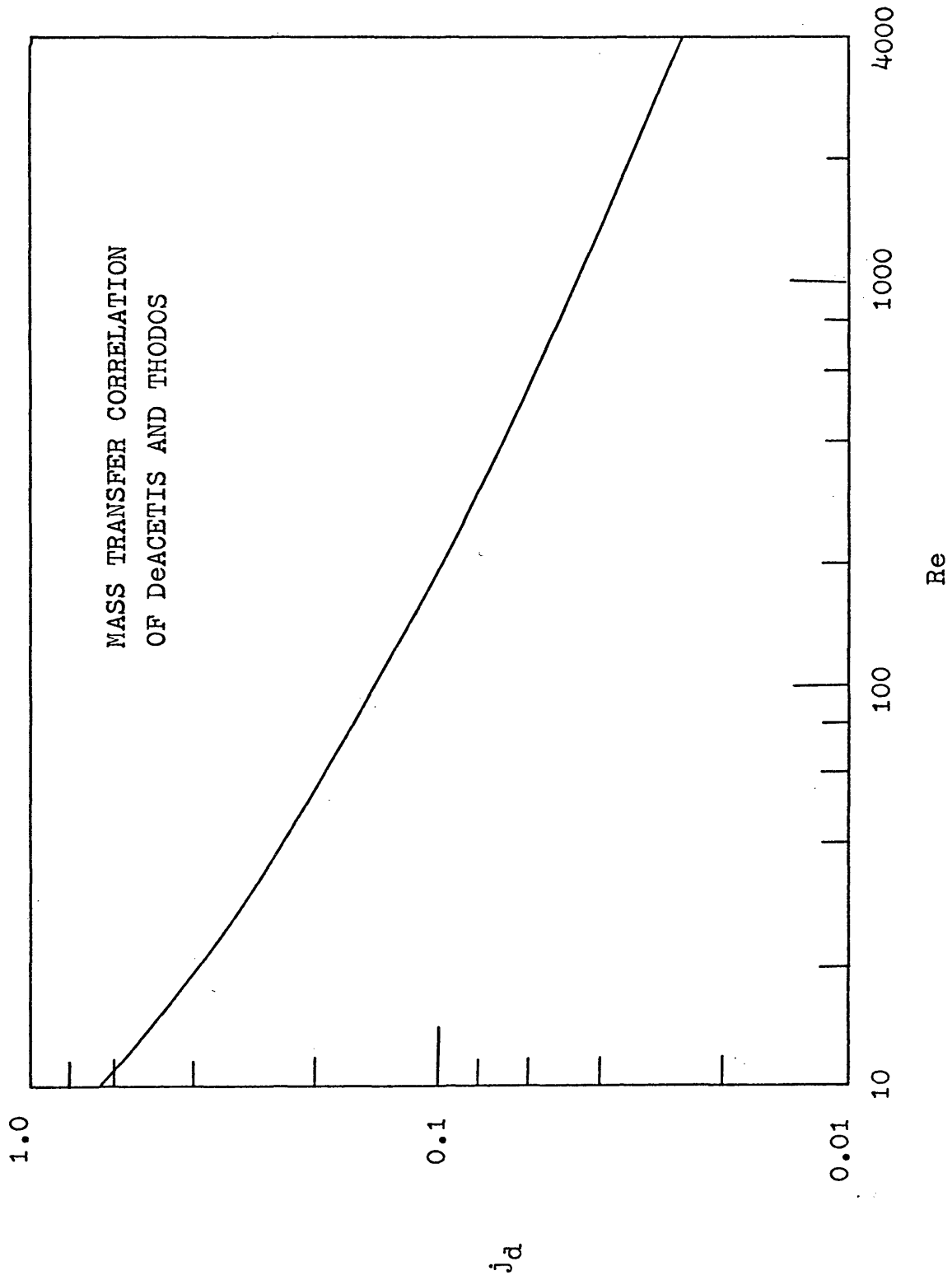


Figure 17. Mass Transfer Correlation

Table 8

CHARCOAL		SYNTHETIC ZEOLITE		SILICA GEL	
$Q/D_p^3 = 2550$		$Q/D_p^3 = 955$		$Q/D_p^3 = 12126$	
System	$\frac{(Fo)(C_o)(Re)(Sc)^{.67}}{(\rho_B/\rho)(v)}$	System	$\frac{(Fo)(C_o)(Re)(Sc)^{.67}}{(\rho_B/\rho)(v)}$	System	$\frac{(Fo)(C_o)(Re)(Sc)^{.67}}{(\rho_B/\rho)(v)}$
CH <sub>4</sub> -H <sub>2</sub>	37.5	CH <sub>4</sub> -H <sub>2</sub>	19.0	CH <sub>4</sub> -H <sub>2</sub>	70.8
" "	40.1	" "	14.6	" "	120.9
" "	40.7	" "	29.9	" "	77.6
" "	40.6	" "	24.6	" "	85.2
N <sub>2</sub> -H <sub>2</sub>	31.8	N <sub>2</sub> -H <sub>2</sub>	12.3		
" "	34.7	" "	18.9		
" "	36.6	" "	21.2		
" "	34.5	" "	10.4		
CH <sub>4</sub> -He	44.6				
" "	44.7				
" "	45.6				
" "	50.2				
N <sub>2</sub> -He	38.6				
" "	42.2				
" "	39.0				
" "	39.0				

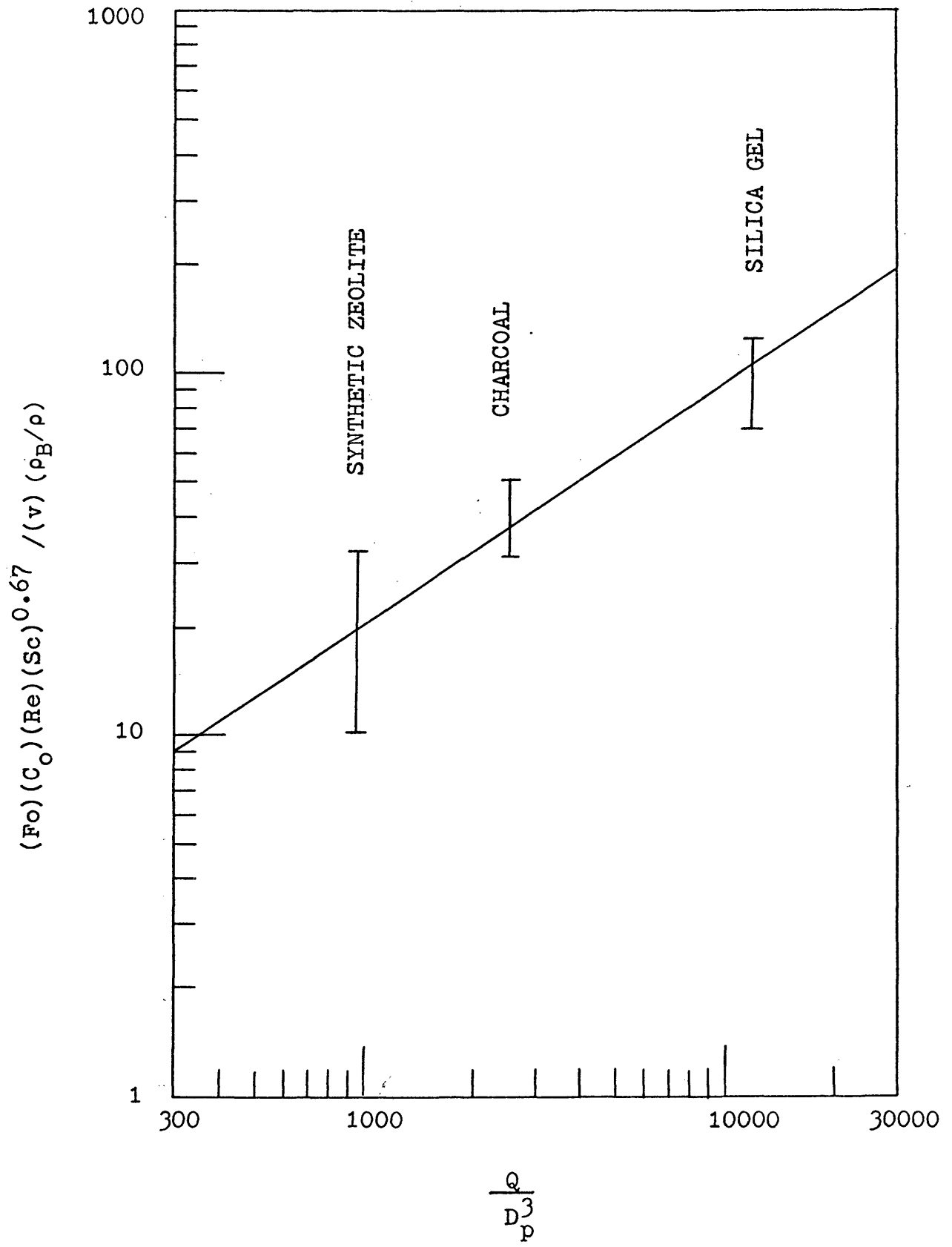


Figure 18. Determination Of The Exponent Of  $\frac{Q}{D_p^3}$

slope of 0.7, and this value is taken to be the exponent of  $Q/D_p^3$ .

Therefore,

$$\frac{(F_o)(C_o)(Re)(Sc)^{0.67}}{(\rho_B/\rho)(v)} \text{ is proportional to}$$

$$\left(\frac{Q}{D_p^3}\right)^{0.7}$$

or

$$F_o = f \left\{ C_o^{-1} Re^{-1} Sc^{-0.67} \frac{\rho_B}{\rho} v \left(\frac{Q}{D_p^3}\right)^{0.7} \right\}$$

Figure 19 shows the final breaktime correlation in the form of a plot of  $F_o$  versus

$$\left\{ (\rho_B/\rho)(v)\left(Q/D_p^3\right)^{0.7} (C_o)^{-1} (Re)^{-1} (Sc)^{-0.67} \right\}.$$

Table 9

For the Determination of the Final Correlation

System	Fo	$\frac{(\rho_B/\rho)(v)(Q/D_p^3)^{0.7}}{(C_o)(Re)(Sc)^{0.67}}$
CH <sub>4</sub> -H <sub>2</sub> on Charcoal	54	349
" " "	161	1050
" " "	1170	7070
" " "	4940	30400
" " "	675	4020
" " "	144	809
" " "	379	2100
" " "	487	2910
" " "	1770	10000
" " "	3240	20400
" " "	755	4480
N <sub>2</sub> -H <sub>2</sub> on Charcoal	624	4750
" " "	54	400
" " "	68	477
" " "	206	1540
" " "	97	656
" " "	575	3800
" " "	110	891
" " "	101	872
" " "	285	2110
" " "	668	4670
" " "	2600	18200

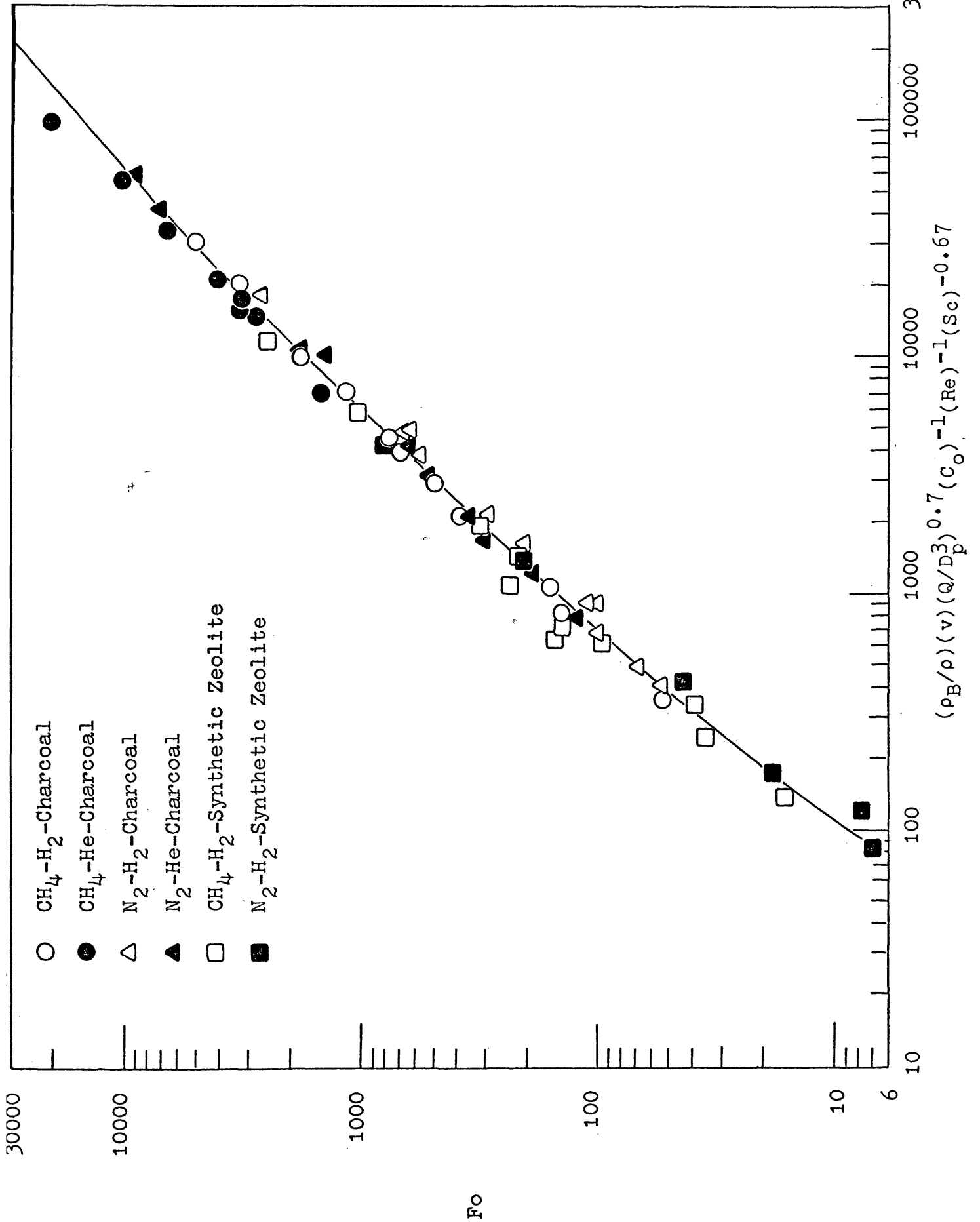
Table 9  
(Continued)

System	Fo	$\frac{(\rho_B/\rho)(v)(Q/D_p^3)^{0.7}}{(C_o)(Re)(Sc)^{0.67}}$
N <sub>2</sub> -He on Charcoal	124	778
" " "	300	1660
" " "	495	3100
" " "	1380	10000
" " "	7090	40700
" " "	191	1190
" " "	362	2050
" " "	659	4090
" " "	1780	10500
" " "	9110	56700
CH <sub>4</sub> -He on Charcoal	3210	17500
" " "	6610	34200
" " "	10200	55200
" " "	3260	16300
" " "	2770	14700
" " "	4040	20900
" " "	19700	97000
" " "	1460	7050
N <sub>2</sub> -H <sub>2</sub> on Synthetic Zeolite	43	426
" " " "	8	118
" " " "	18	170
" " " "	7	82
" " " "	208	1340
" " " "	776	4470

Table 9  
(Continued)

System	Fo	$\frac{(\rho_B/\rho)(v)(Q/D_p^3)^{0.7}}{(C_o)(Re)(Sc)^{0.67}}$
CH <sub>4</sub> -H <sub>2</sub> on Synthetic Zeolite	218	1400
" " " "	97	611
" " " "	39	337
" " " "	155	633
" " " "	1030	5740
" " " "	315	1900
" " " "	243	1050
" " " "	16	137
" " " "	35	237
" " " "	2470	11500
" " " "	144	713





## RESULTS

The breaktimes for the systems considered to determine the correlation are predicted using the curve in Figure 19. These values are listed, and compared with the breaktimes obtained by assuming step-function breakthrough, in Table 10.

The correlation was then tested on systems that were not used in obtaining Figure 19. These systems are:

- 1) Methane-hydrogen on silica gel at  $-115^{\circ}\text{F}$ , reported in Campbell's Ph.D. thesis (1961).
- 2) Water vapor-air on activated alumina at  $80^{\circ}\text{F}$ , reported in Eagleton's Ph.D. thesis (1951).
- 3) Water vapor-air on molecular sieves at  $90^{\circ}\text{F}$ . One run is reported in the literature by Nutter and Burnett (1966, p. 1). It was not possible to acquire a copy of Nutter's Ph.D. thesis which contains other runs.

The breaktimes for the above systems, for selected runs that represent changing conditions, are predicted by using the curve in Figure 19. These predictions are listed and compared with the step-function breakthrough times in Tables 11, 12, and 13.

Table 10  
Prediction of Breaktimes

System	Predicted	Actual	$t_{B\ inst}$	% Error in Prediction	Step-Function Breakthrough
	$t_B$ min	$t_B$ min	min		
CH <sub>4</sub> -H <sub>2</sub> -Charcoal	18	21	31	-14	+48
" "	45	45	63	0	+40
" "	121	116	145	+4	+25
" "	178	163	197	+9	+21
" "	121	120	150	+1	+25
" "	44	51	70	-14	+37
" "	102	110	142	-7	+29
" "	90	90	113	0	+26
" "	220	220	268	0	+22
" "	184	161	197	+14	+22
" "	134	134	170	0	+27
N <sub>2</sub> -H <sub>2</sub> -Charcoal	49	38	53	+29	+40
" "	21	21	31	0	+48
" "	24	24	33	0	+38
" "	70	58	74	+21	+28
" "	38	38	50	0	+32
" "	116	104	124	+12	+19
" "	47	38	64	+24	+68

Table 10  
(Continued)

System	Predicted $t_B$ min	Actual $t_B$ min	$t_{B\ inst}$ min	% Error in Prediction Correlation	Step-Function Breakthrough
N <sub>2</sub> -H <sub>2</sub> -Charcoal	39	30	50	+30	+67
" "	70	59	83	+19	+41
" "	110	92	122	+20	+33
" "	185	148	187	+25	+26
N <sub>2</sub> -He-Charcoal	31	33	40	-6	+21
" "	55	61	70	-10	+15
" "	70	70	78	0	+11
" "	133	102	117	+30	+15
" "	173	170	189	+2	+11
" "	53	53	63	0	+19
" "	69	73	83	-5	+14
" "	96	90	107	+7	+19
" "	125	121	140	+3	+16
" "	180	166	188	+8	+13

Table 10  
Continued)

System	Predicted $t_B$ min	Actual $t_B$ min	$t_B$ inst min	% Error in Prediction Correlation	Step-Function Breakthrough
CH <sub>4</sub> -He-Charcoal	97	97	115	0	+19
" "	124	134	157	-7	+17
" "	116	123	142	-6	+15
" "	226	246	288	-8	+17
" "	163	167	198	-2	+19
" "	107	112	131	-4	+17
" "	210	236	275	-11	+17
" "	211	246	290	-14	+18
N <sub>2</sub> -H <sub>2</sub> Synthetic Zeo.	15	11	22	+36	+100
" "	4	3	9	+33	+200
" "	10	10	27	0	+170
" "	5	5	16	0	+220
" "	32	32	57	0	+78
" "	47	47	73	0	+55

Table 10  
(Continued)

System	Predicted $t_B$ min	Actual $t_B$ min	$t_{B\text{ inst}}$ min	% Error in Prediction Correlation	Step-Function Breakthrough
CH <sub>4</sub> -H <sub>2</sub> -Synthetic Zeolite	55	55	112	0	+104
" "	42	45	102	-7	+127
" "	31	27	81	+15	+200
" "	77	125	210	-38	+68
" "	97	100	167	-3	+67
" "	40	40	74	0	+85
" "	57	84	124	-32	+48
" "	10	12	33	-17	+175
" "	16	19	45	-16	+137
" "	126	148	199	-15	+34
" "	41	53	87	-23	+64

Table 11  
 Prediction of the Breaktime for Methane-Hydrogen  
 On Silica Gel at -115°F System

Co	Re	$\rho_B/\rho$	Sc	Q, ft <sup>3</sup>	D <sub>p</sub> , ft	v lb CH <sub>4</sub> lb solid	Predicted		Actual		% Error in Prediction
							t <sub>B</sub> min	t <sub>B</sub> min	t <sub>B</sub> min	t <sub>B</sub> min	
0.203	4.2	5095	1.6	0.00399	0.007	0.0012	0.92	0.53	1.11	+74	+110
0.606	3.4	5120	1.6	0.00399	0.007	0.0032	1.0	1.0	1.65	0	+65
0.955	13.3	4809	1.6	0.00763	0.007	0.0045	0.34	0.38	0.68	-11	+80
0.852	5.1	5025	1.6	0.00820	0.0059	0.0053	1.40	1.75	2.3	-20	+31
0.455	3.3	5025	1.6	0.00820	0.0059	0.0035	2.7	2.5	3.3	+8	+32
0.852	4.0	5025	1.6	0.00820	0.0059	0.0058	2.0	2.3	2.9	-11	+29

Table 12  
 Prediction of the Breaktime for Water Vapor-Air  
 on Activated Alumina at 80°F

$\frac{C_o}{lb\ H_2O}$ $\frac{lb\ dir}{lb\ dir}$	Re	$\frac{\rho_B}{\rho}$	Sc	Q, ft <sup>3</sup>	D <sub>p</sub> , ft	$\frac{V}{lb\ H_2O}$ $\frac{lb\ solid}{lb\ solid}$	Predicted $t_B$ min	Actual $t_B$ min	$t_B$ inst min	% Error in Prediction Correla- tion	Step-Function Breakthrough
0.00282	13	691	0.6	0.00177	0.0056	0.056	422	426	450	-1	+6
0.00986	13	691	0.6	0.00085	0.0056	0.130	182	108	135	+69	+25
0.00788	13	691	0.6	0.00177	0.0056	0.045	133	100	191	+33	+91
0.00880	6.7	691	0.6	0.00177	0.0056	0.126	551	552	593	0	+7
0.00252	13	691	0.6	0.00165	0.0056	0.050	390	425	466	-8	+10
0.00240	7.2	691	0.6	0.00084	0.0056	0.049	422	401	435	+5	+9
0.00272	4.4	691	0.6	0.00086	0.0056	0.052	681	682	714	0	+5
0.01010	13	691	0.6	0.00339	0.0056	0.145	486	528	570	-8	+8

Table 13  
 Prediction of the Breaktime for Water Vapor-Air  
 On Molecular Sieves at 90°F

$\frac{C_o}{lb\ H_2O}$	Re	$\frac{\rho_B}{\rho}$	Sc	Q, ft <sup>3</sup>	D <sub>p</sub> , ft	$\frac{v}{lb\ H_2O}$	$\frac{lb\ H_2O}{lb\ solid}$	Predicted Actual t <sub>B</sub> min	t <sub>B</sub> min	% Error in Prediction	inst Correla- tion	Step-Function Breakthrough
0.0154	148	596	0.6	0.00357	0.00713	0.225		49	54	64	-9	+19

## DISCUSSION OF RESULTS

It is important to recall that the model assumed for this treatment was that the process is a gas phase mass-transfer controlled, and the solid phase mass transfer coefficient  $k_s$  was assumed to be a function of the inlet concentration  $C_o$ , so that it was not considered as a variable. This places a limitation on the correlation for systems where the above assumption is invalid.

For the methane-helium and nitrogen-helium on charcoal systems, Kidnay and Hiza (1970, p. 953) found the values of  $k_s$  independent of the inlet concentration  $C_o$ . This is in contrast to the behavior of the methane-hydrogen and nitrogen-hydrogen systems studied on the same sample of charcoal by Kidnay (1968, p. 102), where a pronounced concentration dependence was noted. The  $k_s$  values for the helium systems also show a dependence on flow rate  $G$ , again in marked contrast to the hydrogen systems. These results suggest that there is a fundamental difference in the adsorbed phase transport processes between the methane-hydrogen, nitrogen-hydrogen, and the methane-helium, nitrogen-helium systems. This fact plus experimental error (whose magnitude is indicated by the scatter of points in the step-function breakthrough correlation plot in Figure 11), account for the scatter of the points representing the

above four systems, in Figure 19.

The  $k_s$  values for the methane-hydrogen and nitrogen-hydrogen on synthetic zeolite systems are reported, by Kidnay and Hiza (1966, p. 62), to be independent of flow. But these systems account for the biggest scatter of points in the final correlation plot. The step-function breakthrough correlation plot in Figure 20, indicate that experimental error can be the reason for the deviations.

Despite the apparent difference in the adsorbed phase transport processes between the hydrogen and helium systems on charcoal, and the large scatter of points representing the hydrogen systems on synthetic zeolite, the majority of the breaktimes are good for an engineering correlation, and are in nearly all cases, much more accurate than the times predicted by assuming step-function breakthrough, including cases with very steep breakthrough curves such as the helium systems, where reasonably good estimations of the breaktimes can be obtained by assuming step-function breakthrough.

For the methane-hydrogen on silica gel system, Campbell (1961, p. 38) states that this was an internal mass transfer controlled process. This is in contrast to the assumption made in determining the correlation. Despite this fundamental difference, the breaktimes for this system are reasonably well predicted by the correlation, and all are again much more accurate than the times predicted by step-function breakthrough assumption.

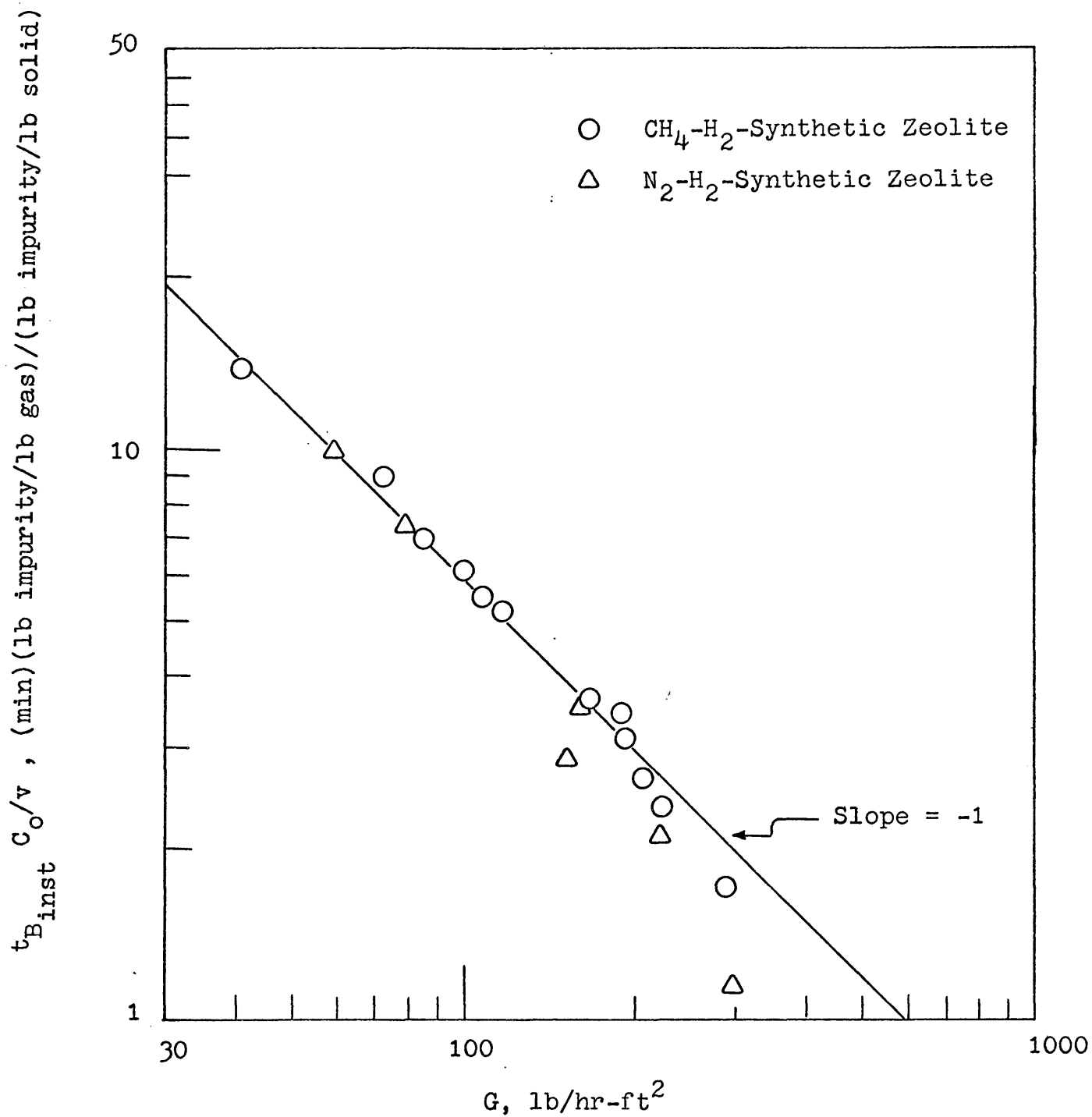


Figure 20. Step-Function Breakthrough Correlation  
For The Synthetic Zeolite Systems

Except for one case in the activated alumina system, all the predicted breaktimes for the water vapor-air systems are satisfactory.

It must be noted that in all the cases, the predicted breaktimes by the correlation would be made much more accurate than the step-function breakthrough times, if the arbitrarily chosen breakpoint was to correspond to a value of  $C/C_0$  less than 0.1. This was not done because the experimental data would be too inexact if a very small value of  $C/C_0$  was tried.

## CONCLUSIONS

A correlation for the breaktime in fixed-bed adsorption systems has been determined by using a dimensional analysis approach. Figure 19 is deemed satisfactory. The scatter of the points is attributed to the assumptions made in the dimensional analysis, approximations made in the determination of the exponents of the variables, and experimental error.

The designer is faced with essentially four choices when predicting the breaktimes:

- 1) Run experiments.
- 2) Use a mathematical approach similar to the method of Eagleton (1951).
- 3) Assume step-function breakthrough.
- 4) Use the correlation.

The last choice is the easiest and the cheapest. It is not highly accurate, but the other methods may not be too much better. Kidnay (1968, p. 103) shows the results of four breakthrough curve calculations using Eagleton's equations. The breaktimes obtained by this method are compared with the predicted breaktimes using Figure 19, and the actual breaktimes, in Table 14.

The main conclusion is that the correlation gives more accurate prediction of breaktimes, than the assumption of step-function breakthrough.

Table 14

A Comparison Between Figure 19  
and the Method of Eagleton

System	Actual $t_B$ (min)	Predicted $t_B$ (min)	
		Correlation	Eagleton's Method
CH <sub>4</sub> -H <sub>2</sub> - Charcoal	45	45	47
" " "	120	121	130
N <sub>2</sub> -H <sub>2</sub> -Charcoal	30	39	34
" " "	148	185	156

## NOTATION

a	= Constant
b	= Constant
c	= Constant
C	= Gas concentration, lb impurity/lb gas
$C_d$	= Gas concentration at the point of discontinuity in the isotherm, lb impurity/lb gas
$C_i$	= Gas concentration at the interface, lb impurity/ lb gas
$C_o$	= Inlet gas concentration, lb impurity/lb gas
d	= Constant
e	= Constant
f	= Constant
$Fo$	= Modified Fourier number $\equiv t_B \mu / \rho D_p^2$
$D_p$	= Effective particle diameter, ft
$D_v$	= Bulk diffusion coefficient, $ft^2/sec$
G	= Mass flow rate based on overall bed cross-section, $lb/hr-ft^2$
$k_g$	= Overall gas film coefficient
$k_s$	= Overall solid film coefficient
L	= Dimension of length
m	= Weight of adsorbent, lb
M	= Dimension of mass
q	= Amount adsorbed, lb adsorbate/lb solid

- Q = Volume of column,  $\text{ft}^3$
- Re = Reynolds number  $\equiv D_p G / \mu$
- S = Surface area of the adsorbent for mass transfer,  
 $\text{ft}^2/\text{lb solid}$
- Sc = Schmidt number  $\equiv \mu / \rho D_v$
- t = Time
- $t_B$  = Breaktime, sec
- $t_{B_{\text{inst}}}$  = Step-function breakthrough time, sec
- v = Adsorbent capacity, lb adsorbate/lb solid
- V = Gas velocity, ft/hr
- X = Weight of the adsorbent, lb
- $\alpha$  = Intercept value of q
- $\beta$  = Slope of the linear adsorption isotherm
- $\mu$  = Viscosity, lb/ft-hr
- $\rho$  = Gas density,  $\text{lb}/\text{ft}^3$
- $\rho_B$  = Bulk density of adsorbent in the adsorption column,  
 $\text{lb adsorbent}/\text{ft}^3$  of column
- $\theta$  = Dimension of time
- $\pi$  = Dimensionless group

## LITERATURE CITED

- Barron, R., 1966, Cryogenic systems: McGraw-Hill Book Co., New York, p. 274-281.
- Bird, R. B., Stewart, W. E., and Lightfoot, E. N., 1960, Transport phenomena: New York, John Wiley and Sons, p. 702-705.
- Campbell, M. L., 1961, Chemical engineering kinetics of physical adsorption: Ph.D. Dissertation, Carnegie Institute of Technology, Pittsburgh, Pa.
- Eagleton, L. C., 1951, Drying of air in fixed beds: Ph.D. Dissertation, Yale University, New Haven, Conn.
- Eagleton, L. C., and Bliss, H., 1953, Drying of air in fixed beds: Chem. Eng. Prog., v. 49, no. 10, p. 543-548.
- Engel, H. C., and Coull, J., 1942, Adsorption studies of vapors in carbon packed towers: Trans. Am. Inst. Chem. Eng., v. 38, p. 947-965.
- Foust, A. S., and others, 1960, Principles of unit operations: New York, John Wiley and Sons, p. 33 and p. 284.
- Hall, K. R., Eagleton, L. C., Acrivos, A., and Vermeulen, T., 1966, Pore and solid diffusion kinetics in fixed bed adsorption under constant pattern conditions: Indus. and Eng. Chemistry Fundamentals, v. 5, no. 2, p. 212-223.
- Hill, T. J., 1948, Statistical mechanics of multimolecular adsorption: Jour. Chem. Phys., v. 16, p. 181.
- Kidnay, A. J., 1968, The purification of hydrogen gas by physical adsorption at 76°K: Ph.D. Dissertation, Colorado School of Mines, Golden, Colo.
- Kidnay, A. J., and Hiza, M. J., 1966, The low temperature removal of small quantities of nitrogen and methane from hydrogen on a synthetic zeolite: Am. Inst. Chem. Eng. Jour., v. 12, no. 1, p. 58-63.

- Kidnay, A. J., and Hiza, M. J., 1970, The purification of helium gas by physical adsorption at 76°K: Am. Inst. Chem. Eng. Jour., v. 16, no. 6, p. 949-954.
- Klotz, I., 1946, The adsorption wave: Chem. Rev., v. 39, p. 241-268.
- Kreith, F., 1967, Principles of heat transfer: Scranton, Penn., International Textbook Co., p. 271-280.
- Langhaar, H. L., 1951, Dimensional analysis and theory of models: New York, John Wiley and Sons, p. 1-45.
- McAdams, W. H., 1942, Heat transmission, 2nd ed.: New York, McGraw-Hill, p. 89.
- Nemeth, J., 1963, Application of the theory of similarity to the study of the kinetics of vapor adsorption: Internat. Chem. Eng., v. 3, no. 1, p. 6-11.
- Nutter, J. I., and Burnet, G., 1963, Drying of air by fixed bed adsorption with molecular sieves: Am. Inst. Chem. Eng. Jour., v. 9, no. 2, p. 202-206.
- \_\_\_\_\_ 1966, Fixed-bed drying of air using molecular sieves: Indus. and Eng. Chemistry Process Design and Devel., v. 5, no. 1, p. 1-5.
- Perry, J. H., ed., 1963, Chemical engineers handbook, 4th ed.: New York, McGraw-Hill.
- Reid, R. C., and Sherwood, T. K., 1958, The properties of gases and liquids, 1st ed.: New York, McGraw-Hill, p. 264-279.
- Satterfield, C. N., and Sherwood, T. K., 1963, The role of diffusion in catalysis: Reading, Mass., Addison-Wesley, p. 31-35.
- Treybal, R. E., 1955, Mass transfer operations: New York, McGraw-Hill, 666 p.
- Vermeulen, T., 1958, Separation by adsorption methods: Advances in Chem. Eng., v. 2, New York, Academic Press, p. 147-208.